1.6. Classical linear crystal optics

By A. M. Glazer and K. G. Cox†

1.6.1. Introduction

The field of classical crystal optics is an old one, and in the last century, in particular, it was the main subject of interest in the study of crystallography. Since the advent of X-ray diffraction, however, crystal optics tended to fall out of widespread use, except perhaps in mineralogy, where it has persisted as an important technique for the classification and identification of mineral specimens. In more recent times, however, with the growth in optical communications technologies, there has been a revival of interest in the optical properties of crystals, both linear and nonlinear. There are many good books dealing with classical crystal optics, which the reader is urged to consult (Hartshorne & Stuart, 1970; Wahlstrom, 1959; Bloss, 1961). In addition, large collections of optical data on crystals exist (Groth, 1906–1919; Winchell, 1931, 1939, 1951, 1954, 1965; Kerr, 1959). In this chapter, both linear and nonlinear optical effects will be introduced briefly in a generalized way. Then the classical derivation of the refractive index surface for a crystal will be derived. This leads on to a discussion on the practical means by which conventional crystal optics can be used in the study of crystalline materials, particularly in connection with mineralogical study, although the techniques described apply equally well to other types of crystals. Finally, some detailed explanations of certain linear optical tensors will be given.

1.6.2. Generalized optical, electro-optic and magneto-optic effects

When light of a particular cyclic frequency ω is incident on a crystal of the appropriate symmetry, in general an electrical polarization **P** may be generated within the crystal. This can be expressed in terms of a power series with respect to the electric vector of the light wave (Nussbaum & Phillips, 1976; Butcher & Cotter, 1990; Kaminow, 1974):

$$P = \sum \varepsilon_o \chi^{(i)} E^i = \varepsilon_o \left(\chi^{(1)} E + \chi^{(2)} E^2 + \chi^{(3)} E^3 + \ldots\right), \quad (1.6.2.1)$$

where the $\chi^{(i)}$ are susceptibilities of order i. Those working in the field of electro-optics tend to use this notation as a matter of course. The susceptibility $\chi^{(1)}$ is a linear term, whereas the higher-order susceptibilities describe nonlinear behaviour.

However, it is convenient to generalize this concept to take into account other fields (*e.g.* electrical, magnetic and stress fields) that can be imposed on the crystal, not necessarily due to the incident light. The resulting polarization can be considered to arise from many different so-called electro-optic, magneto-optic and photoelastic (elasto-optic) effects, expressed as a series expansion of P_i in terms of susceptibilities $\chi_{ijk\ell\ldots}$ and the applied fields **E**, **B** and T. This can be written in the following way:

$$\begin{aligned} P_i = P_i^0 &+ \varepsilon_o \chi_{ij} E_j^{\omega} + \varepsilon_o \chi_{ij\ell} \nabla_\ell E_j^{\omega} + \varepsilon_o \chi_{ijk} E_j^{\omega_1} E_k^{\omega_2} \\ &+ \varepsilon_o \chi_{ijk\ell} E_j^{\omega_1} E_k^{\omega_2} E_\ell^{\omega_3} + \varepsilon_o \chi_{ijk} E_j^{\omega_1} B_k^{\omega_2} \\ &+ \varepsilon_o \chi_{ijk\ell} E_j^{\omega_1} B_k^{\omega_2} B_\ell^{\omega_3} + \varepsilon_o \chi_{ijk\ell} E_j^{\omega_1} T_{k\ell}^{\omega_2} + \ldots . \end{aligned} \quad (1.6.2.2)$$

Here, the superscripts refer to the frequencies of the relevant field terms and the susceptibilities are expressed as tensor components. Each term in this expansion gives rise to a specific effect that may or may not be observed, depending on the crystal symmetry and the size of the susceptibility coefficients. Note a possible confusion: in the notation $\chi^{(i)}$, i is equal to one less than its rank. It is important to understand that these terms describe various properties, both linear and nonlinear. Those terms that describe the effect purely of optical frequencies propagating through the crystal give rise to *linear* and *nonlinear* optics. In the former case, the input and output frequencies are the same, whereas in the latter case, the output frequency results from sums or differences of the input frequencies. Furthermore, it is apparent that nonlinear optics depends on the intensity of the input field, and so is an effect that is induced by the strong optical field.

If the input electrical fields are static (the term 'static' is used here to mean zero or low frequency compared with that of light), the resulting effects are either linear or nonlinear electrical effects, in which case they are of no interest here. There is, however, an important class of effects in which both static and optical fields are involved: linear and nonlinear electro-optic effects. Here, the use of the terms linear and nonlinear is open to confusion, depending on whether it is the electrical part or the optical part to which reference is made (see for example below in the discussion of the linear electro-optic effect). Similar considerations apply to applied magnetic fields to give linear and nonlinear magneto-optic effects and to applied stresses, the *photoelastic* effects. Table 1.6.2.1 lists the most important effects according to the terms in this series. The susceptibilities are written in the form $\chi(\omega_1; \omega_2, \omega_3, \ldots)$ to indicate the frequency ω_1 of the output electric field, followed after the semicolon by the input frequencies $\omega_1, \omega_2, \ldots$.

Table 1.6.2.1. *Summary of linear and nonlinear optical properties*

Type of polarization term	Susceptibility	Effect
P_i^0	$\chi(0; 0)$	Spontaneous polarization
$\varepsilon_o \chi_{ij} E_j^{\omega}$	$\chi(\omega; \omega)$	Dielectric polarization, refractive index, linear birefringence
$\varepsilon_o \chi_{ij\ell} \nabla_\ell E_j^{\omega}$	$\chi(\omega; \omega)$	Optical rotation (gyration)
$\varepsilon_o \chi_{ijk} E_j^{\omega_1} E_k^{\omega_2}$	$\chi(0; 0, 0)$	Quadratic electric effect
	$\chi(\omega; \omega, 0)$	Linear electro-optic effect or Pockels effect
	$\chi(\omega_1 \pm \omega_2; \omega_1, \omega_2)$	Sum/difference frequency generation, two-wave mixing
	$\chi(\omega; \omega/2, \omega/2)$	Second harmonic generation (SHG)
	$\chi(0; \omega/2, \omega/2)$	Optical rectification
	$\chi(\omega_3; \omega_1, \omega_2)$	Parametric amplification
$\varepsilon_o \chi_{ijk\ell} E_j^{\omega_1} E_k^{\omega_2} E_\ell^{\omega_3}$	$\chi(\omega; 0, 0)$	Quadratic electro-optic effect or Kerr effect
	$\chi(\omega; \omega/2, \omega/2, 0)$	Electric-field induced second harmonic generation (EFISH)
	$\chi(-\omega_1; \omega_2, \omega_3, -\omega_4)$	Four-wave mixing
$\varepsilon_o \chi_{ijk} E_j^{\omega_1} B_k^{\omega_2}$	$\chi(\omega; \omega, 0)$	Faraday rotation
$\varepsilon_o \chi_{ijk\ell} E_j^{\omega_1} B_k^{\omega_2} B_\ell^{\omega_3}$	$\chi(\omega; \omega, 0, 0)$	Quadratic magneto-optic effect or Cotton–Mouton effect
$\varepsilon_o \chi_{ijk\ell} E_j^{\omega_1} T_{k\ell}^{\omega_2}$	$\chi(\omega; \omega, 0)$	Linear elasto-optic effect or photoelastic effect
	$\chi(\omega_1 \pm \omega_2; \omega_1, \omega_2)$	Linear acousto-optic effect

† The sudden death of Keith Cox is deeply regretted. He died in a sailing accident on 27 August 1998 in Scotland at the age of 65.

1.6.2.1. *Spontaneous polarization* P_i^0

A spontaneous polarization of a crystal can be created in some polar crystals after a strong static electric field is first applied and then removed. Subsequent application of an electric field in the opposite direction can then reverse the sense of the spontaneous polarization. By analogy with the well known similar phenomenon of ferromagnetism, such crystals are known as ferroelectrics (Jona & Shirane, 1962; Lines & Glass, 1979). This effect is therefore not an optical effect, but is included here for the sake of completeness. For a crystal to be a ferroelectric, it cannot have a centre of symmetry.

1.6.2.2. *Dielectric polarization* $\varepsilon_o \chi_{ij} E_j^\omega$

Application of an electric field **E** of frequency ω to a crystal results in a polarization response whose size depends on the dielectric susceptibility $\chi^{(1)}$. This is a second-rank tensor that is applicable to *all* materials, and is often quoted in terms of the dielectric constant $\varepsilon = \varepsilon_o(1 + \chi)$. For electric fields at optical frequencies, the dielectric constant is equal to the square of the refractive index for light propagating in a certain direction and in a particular polarization state. This effect can only be termed optical if the frequency of the electric field lies at optical frequencies. There is no difference between input and output frequencies, and so the susceptibility is written in the form $\chi_{ij}(\omega; \omega)$. Because there is no change in frequency, this is a linear optical effect.

1.6.2.3. *Optical rotation (gyration)* $\varepsilon_o \chi_{ij\ell} \nabla_\ell E_j^\omega$

This is the phenomenon often known as *optical activity* (Born & Wolf, 1993; Agranovich & Ginzburg, 1984) in which plane-polarized light of frequency ω passing through a medium has its polarization rotated through an angle depending on the path length through the medium. It is seen most easily along uniaxial directions in crystals with the appropriate symmetry. Centrosymmetric crystals cannot show optical rotation. Because no change in frequency occurs, it can be considered to be a linear optical effect.

1.6.2.4. *Quadratic electric effect* $\varepsilon_o \chi_{ijk} E_j^{\omega_1} E_k^{\omega_2}$

If $\omega_1 = \omega_2 = 0$, *i.e.* the susceptibility is $\chi_{ijk}(0; 0, 0)$, the resulting polarization is given by

$$P_i^0 = \varepsilon_o \chi_{ijk} E_j^0 E_k^0.$$

This is therefore a polarization induced in the crystal by a strong static electric field. It is a nonlinear electrical effect, and so it is not an optical property.

1.6.2.5. *Linear electro-optic effect* $\varepsilon_o \chi_{ijk} E_j^{\omega_1} E_k^{\omega_2}$

If $\omega_1 = \omega$ and $\omega_2 = 0$, *i.e.* $\chi_{ijk}(\omega; \omega, 0)$, this contribution becomes

$$P_i^\omega = \varepsilon_o \chi_{ijk} E_j^\omega E_k^0$$

and corresponds to the situation where light of frequency ω passes into the crystal at the same time as a static electric field is applied. The effect, sometimes known as the *Pockels effect*, is to change the polarization state of the incident light, effectively by altering the refractive indices of the crystal. This physical property is governed by the third-rank electro-optic susceptibility $\chi^{(2)}$, components χ_{ijk}, which follow the same symmetry constraints as the piezoelectric tensor. Crystals therefore must lack a centre of symmetry for this effect to be observable. Although this can be classified as a nonlinear effect, because more than one incident field is involved, it is customary to call it a linear electro-optic effect, as only a single electrical field is used, and moreover there is no change in the frequency of the incident light.

1.6.2.6. *Sum/difference frequency generation (two-wave mixing)* $\varepsilon_o \chi_{ijk} E_j^{\omega_1} E_k^{\omega_2}$

It can happen that when two different light fields of frequencies ω_1 and ω_1, such as can be obtained from two lasers, propagate through a crystal, the resulting output frequency can be the sum or difference of the two incident frequencies, through the susceptibility $\chi_{ijk}(\omega_1 \pm \omega_2; \omega_1, \omega_2)$. A particular case is of interest: suppose $\omega_1 = \omega_2 = \omega/2$ *i.e.* $\chi_{ijk}(\omega; \omega/2, \omega/2)$, to get

$$P_i^\omega = \varepsilon_o \chi_{ijk} E_j^{\omega/2} E_k^{\omega/2}.$$

Here, the light, on passing through the crystal, interacts with itself to produce a doubling of the frequency. This important effect is known as *second harmonic generation* or SHG and is used for generating different laser frequencies starting from a fundamental frequency. The observation of SHG is also often a good indicator of the lack of a centre of inversion in a crystal. As two optical fields are involved, the incident field inducing the second one, this is a true nonlinear optical effect.

Another effect can be envisaged in which the susceptibility is $\chi_{ijk}(0; \omega/2, -\omega/2)$, *i.e.* there is a cancellation of the two incident frequencies to produce a polarization in the crystal. This is called *optical rectification*.

Parametric amplification is an effect caused when an incident beam at frequency ω_1 is incident on a nonlinear optical crystal at the same time as an intense pump beam frequency ω_2, where $\omega_2 > \omega_1$. The ω_1 wave is then amplified accompanied by an 'idler' wave of frequency $\omega_3 = \omega_2 - \omega_1$.

1.6.2.7. *Quadratic electro-optic effect* $\varepsilon_o \chi_{ijk\ell} E_j^{\omega_1} E_k^{\omega_2} E_\ell^{\omega_3}$

This effect, known also as the *Kerr effect*, results from setting $\omega_1 = \omega$, $\omega_2 = \omega_3 = 0$, *i.e.* the susceptibility is $\chi_{ijk\ell}(\omega; \omega, 0, 0)$, thus:

$$P_i^\omega = \varepsilon_o \chi_{ijk\ell} E_j^\omega E_k^0 E_\ell^0.$$

Like the linear electro-optic effect described above, a static electric field applied to the medium causes a change in the refractive indices, which then affects the polarization of the transmitted light. The difference here is that the Kerr effect is displayed by all transparent media, including liquids. In an otherwise optically isotropic system, application of a strong static field makes the system optically anisotropic: this change from isotropic to anisotropic can be used to produce a fast optical shutter. Because the light frequency is unchanged, this can be termed a linear optical effect, but on the other hand, because it depends on the square of the static electric field, it is a nonlinear electrical effect.

1.6.2.8. *Electric-field induced second harmonic generation* $\varepsilon_o \chi_{ijk\ell} E_j^{\omega_1} E_k^{\omega_2} E_\ell^{\omega_3}$

If $\omega_1 = \omega_2 = \omega/2$ and $\omega_3 = 0$, *i.e.* the susceptibility is $\chi_{ijk\ell}(\omega; \omega/2, \omega/2, 0)$, the resulting polarization is

$$P_i^\omega = \varepsilon_o \chi_{ijk\ell} E_j^{\omega/2} E_k^{\omega/2} E_\ell^0.$$

A second-harmonic response is obtained, but this time induced by a static electric field. This is called *electric-field-induced SHG* or EFISH. It is a nonlinear optical effect that is created by a linear electric effect.

1.6.2.9. *Four-wave mixing* $\varepsilon_o \chi_{ijk\ell} E_j^{\omega_1} E_k^{\omega_2} E_\ell^{\omega_3}$

One use of a third-order nonlinear optical susceptibility is in the important area of four-wave mixing. In this case, the complex amplitude of the induced polarization at the frequency $\omega_1 = \omega_2 + \omega_3 - \omega_4$ is given by

$$P_i^{\omega_1} = \varepsilon_o \chi_{ijk\ell}(-\omega_1; \omega_2, \omega_3, -\omega_4) E_j^{\omega_2} E_k^{\omega_3} E_\ell^{*\omega_4}.$$

Thus if a nonlinear crystal is pumped by two counter-propagating beams of frequency $\omega_1 = \omega_2 = \omega$, and another beam $\omega_4 = \omega$ is input at some angle, a fourth beam $\omega_3 = \omega$ results whose complex amplitude will be the complex conjugate of the ω_4 beam. Thus four-wave mixing is an important arrangement for producing *phase conjugation*.

1.6.2.10. *Faraday rotation* $\varepsilon_o \chi_{ijk} E_j^{\omega_1} B_k^{\omega_2}$

Application of a static magnetic field to certain crystals through which light of frequency ω passes causes a change in polarization state *via*

$$P_i^{\omega} = \varepsilon_o \chi_{ijk} E_j^{\omega} B_k^0.$$

The effect is to rotate the plane of polarization of the incident light, the size of the effect depending not only on the length of the medium traversed, but also on the size of the applied magnetic field. An interesting difference from ordinary optical rotation is that on reflecting the light beam back through the medium, the plane of polarization is *further* rotated rather than cancelled: this property has been used in making optical isolators.

1.6.2.11. *Quadratic magneto-optic effect* $\varepsilon_o \chi_{ijk\ell} E_j^{\omega_1} B_k^{\omega_2} B_\ell^{\omega_3}$

By analogy with the quadratic electro-optic effect, application of a strong static magnetic field can modulate the polarization state of the incident light *via*

$$P_i^{\omega} = \varepsilon_o \chi_{ijk\ell} E_j^{\omega} B_k^0 B_\ell^0.$$

This effect is also known as the *Cotton–Mouton effect.*

1.6.2.12. *Linear photoelastic effect* $\varepsilon_o \chi_{ijk\ell} E_j^{\omega_1} T_{k\ell}^{\omega_2}$

Also known as the *piezo-optic* effect (or *elasto-optic* effect), this is usually observed through $\chi_{ijk\ell}(\omega; \omega, 0)$, *i.e.* the applied stress is static. Thus the application of a force to an elasto-optic material results in a change in birefringence. This effect can be seen not only in crystals, but also in isotropic materials such as glass or transparent plastics. By observation of a stressed material between crossed polars, the resulting strains can be seen as coloured fringes, a useful way of examining engineering structures.

1.6.2.13. *Linear acousto-optic effect* $\varepsilon_o \chi_{ijk\ell} E_j^{\omega_1} T_{k\ell}^{\omega_2}$

In the acousto-optic effect, the applied stress is at an acoustic frequency ω_2, *i.e.* the relevant susceptibility is $\chi_{ijk\ell}(\omega_1 \pm \omega_2; \omega_1, \omega_2)$. Thus a sound wave passing through an acousto-optic crystal modulates the refractive index *via*

$$P_i^{\omega_1 \pm \omega_2} = \varepsilon_o \chi_{ijk\ell} E_j^{\omega_1} T_{k\ell}^{\omega_2}.$$

A beam of light of frequency ω_1 passing through the crystal can then be diffracted by the refractive index modulation, and so such a crystal is a useful device for converting sound waves into an optical signal for long-distance transmission along optical fibres. As $\omega_1 \gg \omega_2$, the frequency of the input light is only very slightly altered by the sound wave, and for most purposes can be neglected.

1.6.3. Linear optics

1.6.3.1. *The fundamental equation of crystal optics*

It is necessary, in order to understand fully the propagation of light through a general anisotropic crystal, to address the question of the way in which an electromagnetic wave is affected by its passage through a regular array of atoms or molecules. A full analysis of this problem at a microscopical level is complicated and was treated, for example, by Ewald (1916), who showed through consideration of a 'half-crystal' how to link the electromagnetic field outside the crystal to that inside (a good description of Ewald's work on this can be read in the book *P. P. Ewald and his Dynamical Theory of X-ray Diffraction*, published by the International Union of Crystallography, Oxford Science Publications, 1992). For the purposes needed here, it is sufficient to apply Maxwell's equations to a bulk anisotropic continuum crystal, thus taking a macroscopic approach. The treatment here follows that given by Nussbaum & Phillips (1976).

Consider the relationship between the dielectric displacement **D** and an electric field **E** which in tensor terms is given by

$$D_i = \varepsilon_o \varepsilon_{ij} E_j, \tag{1.6.3.1}$$

where ε_o is the vacuum dielectric permittivity and ε_{ij} is a second-rank tensor, the relative dielectric tensor. Correspondingly, there is an induced polarization **P** related to **E** *via*

$$P_k = \varepsilon_o \chi_{k\ell} E_\ell, \tag{1.6.3.2}$$

where $\chi_{k\ell}$ is another second-rank tensor, called the dielectric susceptibility tensor. Note that the restriction to a linear relationship between **D** and **E** (or **P** and **E**) confines the theory to the region of *linear optics*. Addition of higher-order terms (see above) gives *nonlinear optics*. (Nonlinear optics is discussed in Chapter 1.7.)

$$\operatorname{curl} \mathbf{H} = \partial \mathbf{D}/\partial t \tag{1.6.3.3}$$

$$\operatorname{curl} \mathbf{E} = -\partial \mathbf{B}/\partial t, \tag{1.6.3.4}$$

where **B** and **H** are the magnetic induction and magnetic field intensity, respectively. It is customary at this point to assume that the crystal is non-magnetic, so that $\mathbf{B} = \mu_o \mathbf{H}$, where μ_o is the vacuum magnetic permeability. If plane-wave solutions of the form

$$\mathbf{E} = \mathbf{E}_o \exp[i(\mathbf{k} \cdot \mathbf{r} - \omega t)] \tag{1.6.3.5}$$

$$\mathbf{H} = \mathbf{H}_o \exp[i(\mathbf{k} \cdot \mathbf{r} - \omega t)] \tag{1.6.3.6}$$

$$\mathbf{D} = \mathbf{D}_o \exp[i(\mathbf{k} \cdot \mathbf{r} - \omega t)] \tag{1.6.3.7}$$

are substituted into equations (1.6.3.3) and (1.6.3.4), the following results are obtained:

$$\mathbf{k} \times \mathbf{H} = \omega \mathbf{D} \tag{1.6.3.8}$$

$$\mathbf{k} \times \mathbf{E} = -\omega \mathbf{B}. \tag{1.6.3.9}$$

These equations taken together imply that **D**, **H** and **k** are vectors that are mutually orthogonal to one another: note that in general **E** and **D** need not be parallel. Similarly **B** (and hence **H**), **E** and **k** are mutually orthogonal. Now, on substituting (1.6.3.9) into (1.6.3.8),

$$\frac{1}{\mu_o \omega^2} \mathbf{k} \times (\mathbf{k} \times \mathbf{E}) = -\mathbf{D}. \tag{1.6.3.10}$$

Defining the propagation vector (or wave normal) **s** by

$$\mathbf{s} = \frac{c}{\omega} \mathbf{k} = n \hat{\mathbf{s}}, \tag{1.6.3.11}$$

where $\hat{\mathbf{s}}$ is the unit vector in the direction of **s** and n is the *refractive index* for light propagating in this direction, equation (1.6.3.10) then becomes

$$\frac{1}{\mu_o c^2} \mathbf{s} \times (\mathbf{s} \times \mathbf{E}) = -\mathbf{D}. \tag{1.6.3.12}$$

Via the vector identity $\mathbf{A} \times (\mathbf{B} \times \mathbf{C}) = (\mathbf{A} \cdot \mathbf{C})\mathbf{B} - (\mathbf{A} \cdot \mathbf{B})\mathbf{C}$, this result can be transformed to

$$-(\mathbf{s} \cdot \mathbf{s})\mathbf{E} + (\mathbf{s} \cdot \mathbf{E})\mathbf{s} = -\mu_o c^2 \mathbf{D}. \tag{1.6.3.13}$$

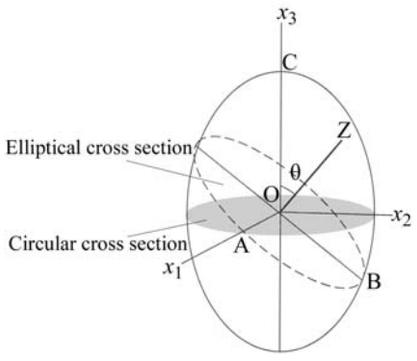

Fig. 1.6.3.1. The optical indicatrix.

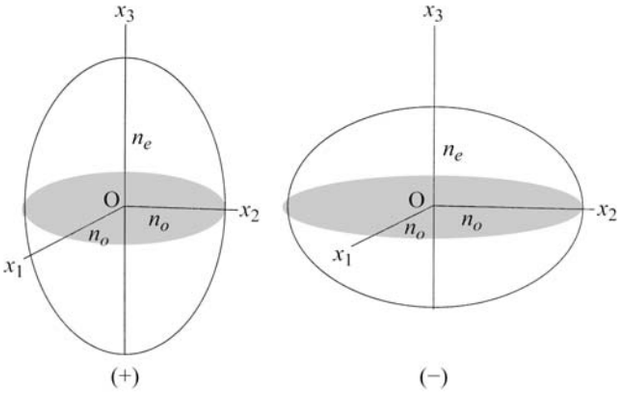

Fig. 1.6.3.2. Positive and negative uniaxial indicatrix.

$\mathbf{s}\cdot\mathbf{s}$ is equal to n^2 and $\mathbf{s}\cdot\mathbf{E}$ can be expressed simply in tensor form as $\sum_j s_j E_j$. Now, with equation (1.6.3.1), the fundamental equation of linear crystal optics is found:

$$\sum_j (\varepsilon_{ihj} + s_i s_j) E_j = n^2 I E_i, \tag{1.6.3.14}$$

where I is the unit matrix.

1.6.3.2. *The optical indicatrix*

Equation (1.6.3.14) is the relevant starting point for the derivation of the way in which light propagates in an anisotropic medium. To solve it in a particular case, treat it as an eigenvector–eigenvalue problem: the E_i are the eigenvectors and n^2 the eigenvalues. For example, take the case of a uniaxial crystal. The dielectric tensor is then given by

$$\begin{pmatrix} \varepsilon_{11} & 0 & 0 \\ 0 & \varepsilon_{11} & 0 \\ 0 & 0 & \varepsilon_{33} \end{pmatrix}. \tag{1.6.3.15}$$

Assume that light propagates along a direction in the x_2x_3 plane, at an angle θ to the x_3 axis. Then, using (1.6.3.11), it is seen that

$$\begin{aligned} s_1 &= 0 \\ s_2 &= n\sin\theta \\ s_3 &= n\cos\theta \end{aligned} \tag{1.6.3.16}$$

and

$$s_i s_j = \begin{pmatrix} 0 & 0 & 0 \\ 0 & n^2\sin^2\theta & n^2\sin\theta\cos\theta \\ 0 & n^2\sin\theta\cos\theta & n^2\cos\theta \end{pmatrix}. \tag{1.6.3.17}$$

Substituting into equation (1.6.3.14) yields

$$\begin{pmatrix} \varepsilon_{11} & 0 & 0 \\ 0 & \varepsilon_{11} + n^2\sin^2\theta & n^2\sin\theta\cos\theta \\ 0 & n^2\sin\theta\cos\theta & \varepsilon_{33} + n^2\cos\theta \end{pmatrix} \begin{pmatrix} E_1 \\ E_2 \\ E_3 \end{pmatrix} = \begin{pmatrix} n^2 & 0 & 0 \\ 0 & n^2 & 0 \\ 0 & 0 & n^2 \end{pmatrix} \begin{pmatrix} E_1 \\ E_2 \\ E_3 \end{pmatrix}. \tag{1.6.3.18}$$

Solving this for the eigenvalues n gives

$$n_1^2 = \varepsilon_{11} \tag{1.6.3.19}$$

as one solution and

$$\frac{1}{n_2^2} = \frac{\cos^2\theta}{\varepsilon_{11}} + \frac{\sin^2\theta}{\varepsilon_{33}} \tag{1.6.3.20}$$

as the other. This latter solution can be rewritten as

$$\frac{1}{n_2^2} = \frac{\cos^2\theta}{n_o^2} + \frac{\sin^2\theta}{n_e^2}, \tag{1.6.3.21}$$

showing how the observed refractive index n_2 varies between the limits set by n_o and n_e, called the *ordinary* and *extraordinary* refractive index, respectively (sometimes these are denoted by ω and ε, respectively). Equation (1.6.3.21) can be thought of as the equation of a uniaxial ellipsoid (circular cross section) with the lengths of the semi-axes given by n_o and n_e. This is illustrated in Fig. 1.6.3.1, where **OZ** is the direction of propagation of the light ray at an angle θ to x_3. Perpendicular to **OZ**, an elliptical cross section is cut from the uniaxial ellipsoid with semi-axes OA equal to n_o and OB given by (1.6.3.21): the directions **OA** and **OB** also correspond to the eigenvectors of equation (1.6.3.4).

Direction **OA** is therefore the direction of the electric polarization transverse to the propagation direction, so that the refractive index measured for light polarized along **OA** is given by the value n_o. For light polarized along **OB**, the refractive index would be given by equation (1.6.3.7). When **OZ** is aligned along x_3, a circular cross section of radius n_o is obtained, indicating that for light travelling along **OZ** and with any polarization the crystal would appear to be optically isotropic. The ellipsoid described here is commonly known as the *optical indicatrix*, in this case a *uniaxial indicatrix*.

Two cases are recognized (Fig. 1.6.3.2). When $n_o < n_e$, the indicatrix is a prolate ellipsoid and is defined to be positive; when $n_o > n_e$, it is oblate and defined to be negative. Note that when $n_o = n_e$ the indicatrix is a sphere, indicating that the refractive index is the same for light travelling in any direction, *i.e.* the crystal is optically isotropic. The quantity $\Delta n = n_e - n_o$ is called the *linear birefringence* (often simply called *birefringence*). In general, then, for light travelling in any direction through a uniaxial crystal, there will be two rays, the ordinary and the extraordinary, polarized perpendicular to each other and travelling with different velocities. This splitting of a ray of light into two rays in the crystal is also known as *double refraction.*

The origin of the birefringence in terms of the underlying crystal structure has been the subject of many investigations. It is obvious that birefringence is a form of optical anisotropy (the indicatrix is not spherical) and so it must be linked to anisotropy in the crystal structure. Perhaps the most famous early study of this link, which is still worth reading, is that of Bragg (1924), who showed that it was possible to calculate rough values for the refractive indices, and hence birefringence, of calcite and aragonite. His theory relied upon the summation of polarizability contributions from the Ca^{2+} and O^{2-} ions.

Returning now to the theory of the indicatrix, more general solution of the fundamental equation (1.6.3.14) leads to a triaxial

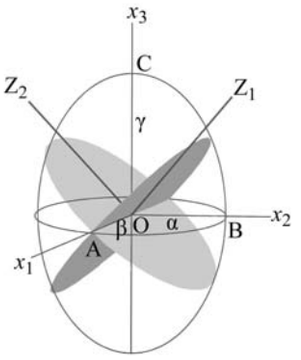

Fig. 1.6.3.3. Biaxial indicatrix, showing the two optic axes and corresponding circular cross sections.

ellipsoid, *i.e.* one in which all three semi-axes are different from one another (Fig. 1.6.3.3).

It is conventional to label the three axes according to the size of the refractive index by $n_\gamma > n_\beta > n_\alpha$ (or simply $\gamma > \beta > \alpha$). In such an ellipsoid, there are always two special directions lying in the γ–α plane, known as the *optic axial plane*, and perpendicular to which there are circular cross sections (shown shaded) of radius β. Thus these two directions are optic axes down which the crystal appears to be optically isotropic, with a measured refractive index β for light of any polarization. For this reason, crystals with this type of indicatrix are known as *biaxial*. When the angle between the optic axes, denoted conventionally as $2V$, is acute about the γ axis, the crystal is *positive biaxial*, and when it is acute about α the crystal is *negative biaxial*. Note that as $2V$ becomes smaller, the biaxial indicatrix becomes closer to a uniaxial indicatrix (positive or negative). In all general directions the crystal is optically anisotropic. Thus, for light along x_3, the measured refractive indices will be α and β for light polarized along x_1 and x_2, respectively; for light along x_2, α and γ are measured for light polarized along x_1 and x_3, respectively; and along x_1, β and γ are measured for light polarized along x_2 and x_3, respectively. There are therefore three different linear birefringences to measure: γ–β, β–α and γ–α.

The different indicatrices are oriented in the crystal according to symmetry considerations (Table 1.6.3.1), and so their observation can form valuable and reliable indicators of the crystal system.

1.6.3.3. *The dielectric impermeability tensor*

It has been seen how the refractive indices can be described in a crystal in terms of an ellipsoid, known as the indicatrix. Thus for orthogonal axes chosen to coincide with the ellipsoid axes, one can write

$$\frac{x_1^2}{n_1^2} + \frac{x_2^2}{n_2^2} + \frac{x_3^2}{n_3^2} = 1, \qquad (1.6.3.22)$$

where $n_1 = (\varepsilon_{11})^{1/2}$, $n_2 = (\varepsilon_{22})^{1/2}$ and $n_3 = (\varepsilon_{33})^{1/2}$. One can write this equation alternatively as

$$\eta_{11}x_1^2 + \eta_{22}x_2^2 + \eta_{33}x_3^2 = 1, \qquad (1.6.3.23)$$

where the $\eta_{ii} = 1/\varepsilon_{ii}$ are the *relative dielectric impermeabilities*. For the indicatrix in any general orientation with respect to the coordinate axes

$$\eta_{11}x_1^2 + \eta_{22}x_2^2 + \eta_{33}x_3^2 + 2\eta_{12}x_1x_2 + 2\eta_{23}x_2x_3 + 2\eta_{31}x_3x_1 = 1. \qquad (1.6.3.24)$$

Thus the dielectric impermeability tensor is described by a second-rank tensor, related inversely to the dielectric tensor.

1.6.4. Practical observation of crystals

1.6.4.1. *The polarizing microscope*

There are countless applications of polarizing microscopy. One of the largest fields of use is in mineralogy and petrology, where the requirement is to identify naturally occurring minerals, the optical properties of which have already been determined elsewhere. Medical applications of a similar sort exist, for instance in the identification of the minerals present in bladder or kidney stones. The chemist or materials scientist who has synthesised a crystalline material may also wish to identify it from known properties, or it may be a new substance that needs to be described. For other purposes it might, for example, be necessary to determine the orientation (relative to crystallographic axes) of mineral specimens, *e.g.* in the cutting of synthetic corundum for the manufacture of watch jewels. This section explains the point of view of an observer who wishes to record and measure optical properties, for whatever reason. Although much of what follows is discussed in terms of mineral crystals, it is equally valid for crystals in general, whether organic or inorganic.

The polarizing microscope incorporates five major features not found in ordinary microscopes. These are:

(i) A *polarizer*, normally a sheet of Polaroid, which is part of the microscope substage assembly. This produces plane-polarized light before the light reaches the specimen. In some microscopes, the polarizer can be rotated, though applications of this technique are rare. In the commonly used petrological microscope, the vibration direction of the polarizer is set in what is called the E–W direction, that is, as the user of the microscope sees the field of view, the vibration direction is from side to side.

(ii) An extra, high-power *condenser* situated in the substage immediately below the specimen. The condenser is switched in and out of the optical path as required.

(iii) A *rotating stage*, circular in plan and graduated in degrees. For a number of purposes, specimens can be rotated through known angles.

(iv) An *analyser*, a second polarizing device, situated in the microscope tube above the specimen. Its vibration direction is set at right angles to that of the polarizer, *i.e.* usually N–S. Like the condenser, this can be inserted into the optical path as needed.

(v) A *Bertrand lens*, also in the microscope tube and insertable as required, which has the function of transferring images from the back (upper) focal plane of the objective to the front (lower) focal plane of the eyepiece. The Bertrand lens and the extra substage condenser are used together to convert the microscope from the *orthoscopic* to the *conoscopic* configuration (see later).

In addition, polarizing microscopes have slotted tubes that allow the insertion of a variety of extra devices generally known as accessory plates. Most common amongst these are the sensitive-tint plate (or 1λ plate) and the quartz wedge.

Objective lenses of various magnifying powers are mounted in a rotating turret. Apart from magnification (typically *ca* ×5 for low power, and ×40 or more for high power), the *numerical aperture* (n.a.) of a lens is an important feature. This is defined as the diameter divided by the focal length. This is a measure of the angle of the cone of light that can enter the objective. In the

Table 1.6.3.1. *Symmetry constraints on the optical indicatrix*

Crystal system	Indicatrix	Orientation constraints
Cubic	Isotropic (sphere)	None
Tetragonal Trigonal Hexagonal	Uniaxial	Circular cross section perpendicular to **c**
Orthorhombic	Biaxial	All indicatrix axes aligned along **a**, **b** and **c**
Monoclinic	Biaxial	One indicatrix axis aligned along **b** (second setting)
Triclinic	Biaxial	None

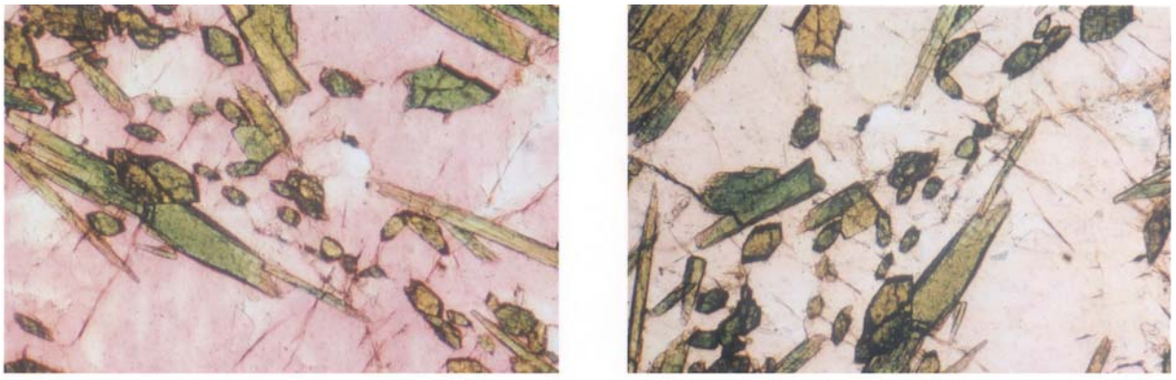

(*a*) (*b*)

Fig. 1.6.4.1. A thin section of a rock containing the minerals aegirine (elongated crystals) and eudyalite (the matrix) viewed in plane-polarized light in two positions at right angles to each other [(*a*) and (*b*)]. Aegirine shows pleochroism from grass-green to yellow–green (compare specific crystals in the two photographs). Eudyalite shows pleochroism from pink to almost colourless.

conoscopic use of the microscope (see Section 1.6.4.11), this angle is required to be as large as possible so that the properties of rays travelling through the crystal in a variety of directions can be observed. Numerical apertures of more than *ca* 0.9 can not be achieved with 'dry' objectives, but higher values are obtained by inserting a drop of immersion oil between the specimen and the lens.

Eyepieces in polarizing microscopes are set in a short tube, at the lower end of which is mounted a set of cross wires, which lie in the front focal plane of the lens. When the microscope is properly focused, a real image of the specimen, created by the objective, is made to coincide with the cross wires. The cross wires are conventionally oriented vertically (N–S) and horizontally (E–W) in the field of view, and coincide with the vibration directions of the polarizer and analyser.

1.6.4.2. *Specimen preparation*

Specimens for examination with the polarizing microscope are usually of two different sorts: collections of small crystals or grains (and individual crystals), and thin sections cut from larger solid samples. In the first category, the material is often crushed to a fine sand, scattered on a microscope slide, a drop of immersion oil is applied, and a cover slip is placed on top. For special applications, an individual crystal may, for example, be mounted on the end of a glass fibre, and similarly examined under immersion oil. The thin-section technique is more widely used in petrology. Here a rock sample is cut into a section of standard thickness (0.03 mm) and mounted on a glass slide, using a resinous mounting material, formerly Canada Balsam but now synthetic. Small single crystals can also be used by mounting them on a spindle stage, or similar device, which allows one to orient the crystal in the microscope.

1.6.4.3. *The indicatrix as an aid to practical microscopy*

It is convenient for the microscopist to imagine the indicatrix sitting inside the crystal under observation. The indicatrix ellipsoid is fixed with respect to the crystallographic axes, according to different crystal systems (Table 1.6.3.1). The radial dimensions of the ellipsoid, in whatever direction, are a measure of the refractive index of a ray vibrating in that direction. Hence, because ray directions are approximately parallel to the microscope axis, a planar section across the indicatrix at right angles to the axis approximately contains the vibration directions of the ray. Such a section is in general an ellipse, the magnitudes of the major and minor axes of which represent the relative refractive indices, and the directions of which represent the vibration directions of the two transmitted rays. In all cases, the ray with the greater refractive index is known as the *slow ray* and the other as the *fast ray*. In uniaxial crystals the ordinary ray may be slow or fast, depending on the optic sign. This mental image of the indicatrix acts as the microscopist's guide in the practical operations that follow.

1.6.4.4. *Vibration directions*

For the microscopist, the overriding feature of the behaviour of light transmitted through crystals is double refraction. Many of the observations that can be made with the polarizing microscope depend on the ability to distinguish the *individual* properties of the two rays. In general, they have different refractive indices, and in coloured crystals they may show different absorptions (*i.e.* the rays show different colours after transmission, the phenomenon known as *pleochroism* – see Fig. 1.6.4.1).

When the microscope is used for observations in *plane-polarized* light, the polarizer is inserted into the optical path but the analyser is not. The light before entering the crystal is polarized E–W. On entry, in the general case where the vibration directions of the crystal happen to lie in a random orientation relative to the vibration direction of the polarizer, the light is transmitted as two rays resolved into the two vibration directions of the specimen. These reach the observer's eye unchanged, and the effects observed are an average of what each ray would individually demonstrate.

Two cases can be used to illustrate this fundamental concept. The mineral calcite ($CaCO_3$) is always given as an example of extreme double refraction. In sections cut parallel to the *c* crystallographic axis, the two rays have refractive indices of 1.486 and 1.658, and this is the maximum difference they can show. Crystals in other orientations always show a smaller difference. The numerical difference between the two refractive indices, when we have identified the maximum difference, is what is quoted as the *birefringence* of the mineral, and for calcite it is unusually large (0.172) by the standards of other commonly occurring minerals (*cf.* quartz = 0.009). Birefringence is an important quantitative optical property, because in thin sections it is easily measurable. It is also useful to refer to the birefringence of individual grains, but this should not be confused with the use of the same term, based on maximum birefringence, as a diagnostic optical property of the material concerned.

Consider a calcite crystal lying with its *c* axis in the plane of the microscope slide. The vibration directions are parallel and at right angles to the crystallographic axis. On rotation of the stage, the *c* axis may be brought into parallelism with the vibration direction of the polarizer, in which case all the light is transmitted using only one of the vibration directions, which in this case has a refractive index of 1.486. On turning the stage through a right angle, all the effects seen are completely due to the other ray, with a refractive index of 1.658. The mounting medium in standard thin-section preparations has a refractive index of *ca* 1.54.

Hence, in the first position there is quite a large contrast between the refractive index of the crystal grain and the mounting medium, and in the other it is considerably smaller. Calcite is usually a highly transparent and virtually colourless substance, and whether the observer can even see the crystals depends on the refractive index difference between it and the mounting medium. In the first case, it is highly visible and in the second case it is harder to see. It is of course the roughness of the surface of the thin section, or the angularities of the form of the crushed crystal, which create small refractions, if there is a refractive-index contrast between it and the mounting medium, and thus make the crystal visible. The general property is known as *relief*. High relief means highly visible in this sense. Calcite shows such extreme changes in relief on rotation of the stage that the phenomenon is known as *twinkling*. Relief is not a measurable property, but to the experienced microscopist it is a subtle and useful guide to identification.

As a second example consider the mineral biotite, which shows extremely strong pleochroism. Biotite is for practical purposes a hexagonal mineral having a platy form dominated by a strong cleavage on (001.1). In thin sections, biotite crystals cut across the cleavage, *i.e.* parallel to the direction [00.1], are typically very dark brown in plane-polarized light when the cleavage lies parallel to the polarizer direction. When turned through 90°, the same crystals are only a very pale brown, pale yellow, or almost colourless. The colour contrast, a consequence of the different absorbing properties of the two rays, is striking. Examples of pleochroism are shown in Fig. 1.6.4.1.

From these examples it should be clear that the different rays show different things. However, the microscopist needs to be certain that the observations made refer exactly to one ray or the other. When the analyser is inserted into the optical path, most crystals (excluding those of the cubic system, and crystallites lying in special orientations) will show *polarization colours*, a consequence of the interference between the two rays once they are recombined vibrating in the analyser plane. Details will be discussed below, but for the present purpose it is the *extinction position* that is of importance. On rotation, a crystal viewed with both analyser and polarizer in position (a configuration known as *crossed Nicols*, after the Nicol prism, the forerunner of Polaroid) will transmit no light in two positions at right angles to each other. This happens when the vibration direction of a transmitted ray coincides with that of the polarizer. In this case, all the light transmitted through the crystal vibrates in a single direction, at right angles to the vibration direction of the analyser, and it is consequently unable to reach the observer. Thus, for all observations of the effects of a particular ray, crossing the polars (inserting the analyser), turning the stage to an extinction position, and then uncrossing the polars (removing the analyser) leaves the specimen showing the pure effects of whichever ray vibrates in the same direction as the polarizer. Much that follows depends on this simple operation.

1.6.4.5. *Measuring refractive indices*

Refractive indices measured carefully can be extremely useful aids in crystal identification, as well as being of importance as physical properties of interest. Apart from distinguishing crystalline species that may look similar under the microscope but have widely different refractive indices, the precise composition of crystalline materials belonging to important solid-solution series (*e.g.* the plagioclase feldspars or the olivines, in geological applications) can also be determined.

The direct measurement of refractive indices is often made by the examination of crystal grains mounted in an immersion oil, using the so-called *Becke line* test. This is observed in plane-polarized light with the substage diaphragm closed down to produce a narrow beam of essentially parallel rays. A medium-power lens is usually suitable. When the oil has a refractive index different from that of the crystal, the Becke line appears as a bright rim of light around the edge of the crystal. However, as the microscope tube is racked up and down slightly (*i.e.* the position of focus is changed), the Becke line moves in or out relative to the crystal edge. As the position of focus is *lowered* the line moves towards the medium with the *lower* refractive index, *e.g.* if the oil has a higher refractive index than the crystal, lowering the focus (racking down) causes the Becke line to contract into the crystal. It is of course important to set the specimen in an extinction position before making the observation. If the oil has a refractive index between those of the two rays passing through the crystal, then the behaviour of the Becke line will reverse if the crystal is rotated to the other extinction position. In cases where there is a very large contrast between the crystal and the surrounding medium, a line as such may not be observed, but rather the specimen may appear to glow with concentrated light. The equivalent of Becke line movement is then the expansion or contraction of the light pool with changing focus.

The general objective of the observations is eventually to achieve an exact match between the immersion medium and the crystal. This is done by choosing different oils, or mixtures of oils, in sequence, the refractive indices of which are measured by a suitable refractometer. Ideally monochromatic or near-monochromatic light (*e.g.* the Na doublet with $\lambda = ca$ 590 nm) is used, in which case the Becke line simply disappears when the crystal and the oil match. In white light however, because of dispersion by the oil, a match is shown by the presence of *two* faint Becke lines, one red and one greenish blue, which migrate in opposite directions as the focus is changed.

The general strategy of refractive-index determination is perfectly straightforward for cubic crystals, but requires the separate determination of values of n_e and n_o in uniaxial crystals, and n_α, n_β and n_γ in biaxial crystals. The most general case is that of the biaxial crystal. If a large number of crystal grains in the mount are examined, a number of cases may be distinguished.

(i) All grains have both refractive indices higher than the oil. The oil has a refractive index below n_α.

(ii) All grains have both refractive indices below that of the oil. The oil has a refractive index above n_γ.

(iii) Some grains have both refractive indices above that of the oil, while others have one above and one below. The oil has a refractive index between n_α and n_β.

(iv) Conversely, some grains have both refractive indices below the oil, while others have one above and one below. The oil has a refractive index between n_β and n_γ.

Uniaxial crystals present a simpler series of cases, in which the crystal may show both refractive indices higher than the oil (*i.e.* the refractive index of the oil is less than that of the fast ray), both lower than the oil, or one higher and one lower.

Systematic application of the above techniques leads to the determination of all the refractive indices required, and constitutes one of the most powerful methods of crystal identification or description. However, it is useful to make an additional check using the fact that, in anisotropic crystals, any specimen that fails to show polarization colours between crossed polars (*i.e.* remains dark in all stage positions) must lie with an optic axis parallel to the microscope axis. Such a crystal directly shows n_o (uniaxial crystals) or n_β (biaxial crystals). Furthermore, crystal grains showing maximum birefringence (see below) can be checked to see if they give a centred flash figure (see later), and if they do, their two vibration directions will show n_e and n_o, or n_α and n_γ, that is, the optic axis or axes lie in the plane of the microscope slide.

In larger crystalline specimens, several other techniques are available for measuring the refractive index. Perhaps the simplest and also the most convenient is to cut the crystal into a prism, and use minimum-deviation measurements on a spectrometer table. In addition, large plates can be inserted directly into a commer-

cial refractometer, in order to measure the refractive index directly.

1.6.4.6. *Determination of linear birefringence*

The numerical determination of linear birefringence gives less information than a full set of refractive-index measurements, but is nevertheless highly useful in crystal identification, particularly in mineralogical and petrological applications where the thin section is the norm. It is also a most sensitive indicator of changes in the crystal structure at a phase transformation or as a function of temperature, pressure *etc.* Refractive-index determination is tedious, but birefringence determination is quick and easy.

Double refraction generates polarization colours when crystals are viewed between crossed polars, except where the crystal is by chance in an extinction position, or cut normal to an optic axis. The colours result from the interference of the two transmitted rays when they are combined into one vibration direction in the analyser. Polarization colours are best observed with the substage diaphragm moderately closed down, so that the transmitted light corresponds to a roughly parallel bundle of rays (if the diaphragm is wide open, and the supplementary condenser is inserted, the resultant rays are far from parallel, and the polarization colours will immediately be seen to degrade in the direction of whitening).

Considering a section showing two refractive indices, n_1 and n_2, the time difference required for a ray to traverse the section is

$$t = \frac{nz}{c}, \tag{1.6.4.1}$$

where z is the thickness of the section. The time difference between the two rays is then

$$t_1 - t_2 = \frac{(n_1 - n_2)z}{c}, \tag{1.6.4.2}$$

which is referred to as the *retardation*. Multiplication by c gives the *relative retardation* or *optical path difference*, R, where

$$R = c(t_1 - t_2) = (n_1 - n_2)z. \tag{1.6.4.3}$$

R is usually expressed in nm (formerly mμ).

The possibilities of interference clearly depend on R, but also on wavelength. For complete destructive interference, because of the way the transmitted rays are resolved into the vibration direction of the analyser (see Fig. 1.6.4.2), R must either be zero (as in cubic crystals, and sections normal to optic axes in anisotropic crystals) or a whole number of wavelengths. Thus as R changes, either with thickness, orientation of the crystals or with variation in birefringence in different substances, a variety of colours are produced, essentially formed from white light with various wavelengths *subtracted.* There is a good discussion of this point in Wahlstrom (1959).

Fig. 1.6.4.3 shows the effect of increasing R on a variety of visible-light wavelengths. When R is zero, no light is transmitted since all wavelengths show total destructive interference. As R increases a little, all wavelengths continue to show interference, and the polarization colours are essentially greys, which decrease in darkness until the middle of the first order where the grey is very pale, almost white. Most wavelengths at this stage are showing relatively strong transmission. With increasing R, the region is reached where the shortest wavelengths of the visible light spectrum (violet) are beginning to approach a phase difference of 1λ. The transmitted light then takes on first a yellow tinge and then bright orange, as violet light (at $R \approx 400$ nm) and then blue are completely removed. Next, the removal of green light ($R \approx 500$ nm) results in the transmitted light being red and at $R \approx 560$ nm the top of the *first-order* colours is reached with the removal of yellow light. The resultant polarization colour is a distinctive magenta colour known as sensitive tint. The accessory plate known as the 'sensitive-tint' or '1λ' plate is made to have $R = 560$ nm. Its use will be explained below, but meanwhile note that the polarization colour is so-called because with only very slight changes in R it becomes obviously red (falling R) or blue (rising R).

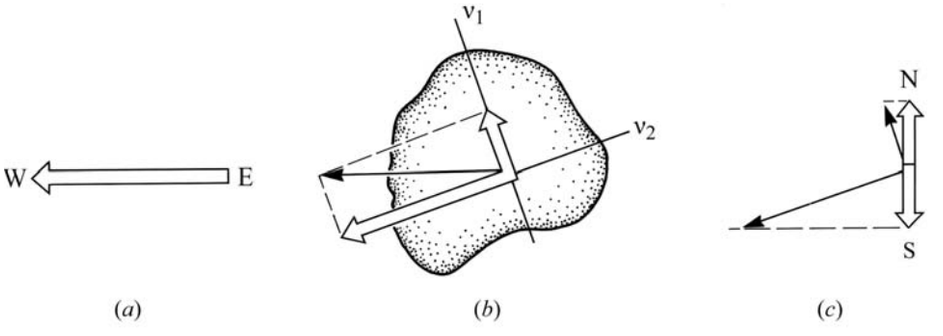

Fig. 1.6.4.2. Successive sections across the optical path of the microscope. (*a*) Above the polarizer, beneath the crystal. Polarized light vibrates E–W. (*b*) Within the crystal. Transmitted light is resolved into the two vibration directions of the crystal (ν_1 and ν_2). (*c*) Above the analyser. The two transmitted rays are resolved into the N–S direction. Amplitudes are shown, but phase difference is not.

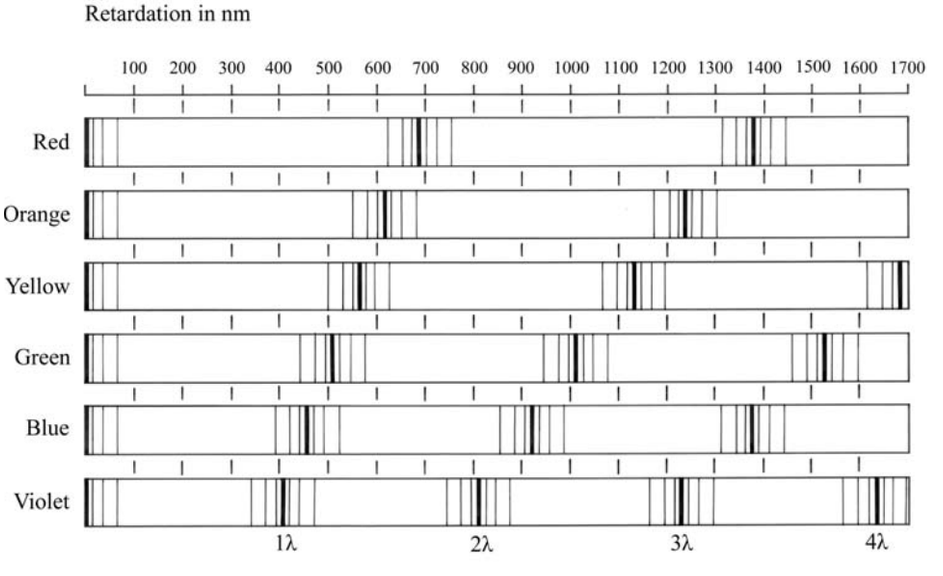

Fig. 1.6.4.3. Plot of retardation, R, *versus* wavelength, showing how polarization colours are formed.

Between $R = 560$ nm and $R = 1120$ nm, the second-order colours are produced, and are similar in appearance to the colours of the rainbow (blue, green, yellow, orange and red in sequence), as orange, red, violet, blue, and green are successively cut out. The *third-order* colours ($R = 1120$–1680 nm) are essentially a repeat of the second-order, but there is a subtle change of quality about them, as they take on slightly garish hues compared with rainbow colours (the red at the top of the order has for example a distinct air of 'shocking pink' or even lipstick about it). This effect is a consequence of the increasing chances that two wavelengths

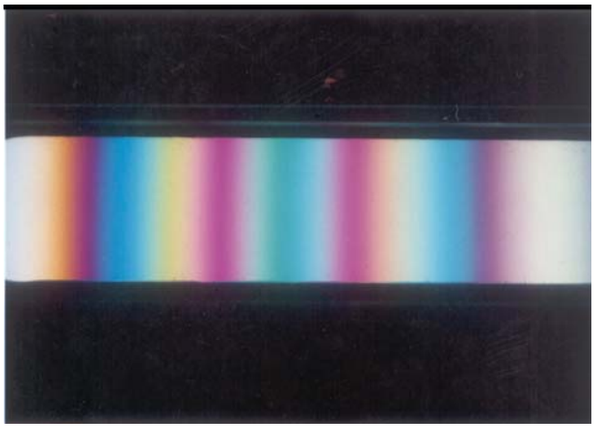

Fig. 1.6.4.4. A quartz wedge between crossed Nicols. The thin end is on the left. The colours shown vary between about the middle of the first order up to high fifth order.

will be cut out simultaneously (see Fig. 1.6.4.3), *e.g.* while first-order red results from the removal of green, second-order red results from the removal of both violet and yellow.

With increasing R, the distinction of colours within each order becomes weaker as the number of wavelengths simultaneously removed increases. Colours are diluted towards grey or white, so that from the fifth order upwards the range is little more than an alternation of pale pinkish and pale greenish tints. Eventually, at higher orders the polarization colours become a more-or-less uniform dull white. Fig. 1.6.4.4 shows the colours produced by a quartz crystal cut into a wedge shape.

1.6.4.7. *Identification of polarization colours*

Birefringence can be determined quantitatively if the polarization colour can be correctly identified, and the section is of known thickness (see Fig. 1.6.4.6). It is of course necessary to distinguish between the birefringence of an individual grain, which will depend on orientation (see Fig. 1.6.4.5*a*), and the maximum birefringence (highest polarization colour) shown by the crystals concerned. It is the latter that is diagnostic, and in general it will be necessary to examine as many grains as possible to determine it.

The grey colours of the lower part of the first-order colours are unique and immediately identifiable, but all other colours are at least superficially ambiguous. Even first-order white may be confused with a high-order white. There are essentially two methods of determining the order of an ambiguous colour, the first of which, fringe counting, is discussed here. Other methods depending on the use of the quartz wedge and sensitive-tint plate will be considered later.

1.6.4.8. *Fringe counting*

In a well made thin section, most crystals show a uniform polarization colour because of uniform orientation and thickness. Crystal edges, however, frequently taper off to near-zero thickness. In this case, the edge acts as a natural wedge of variable R and displays a series of fringes corresponding to the orders within the complete spectrum of interference colours, from first-order grey up to the main colour shown by the body of the crystal (Figs. 1.6.4.5*b* and *c*). Using a moderately high power objective, it is often easy to identify the individual bands and thus count up to the order concerned. The colour band red–sensitive tint–blue

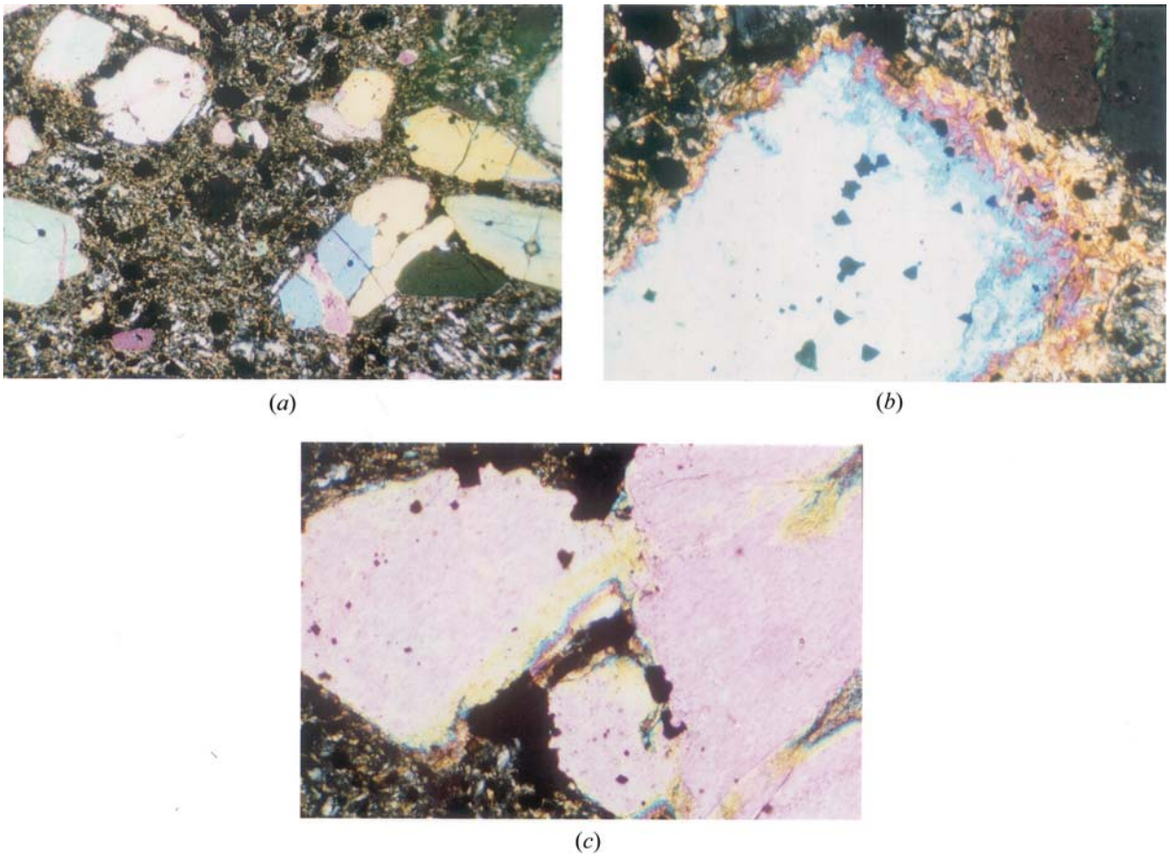

Fig. 1.6.4.5. (*a*) Photomicrograph between crossed polars of a thin section of rock containing large olivine crystals set in a fine-grained matrix. The olivine crystals show a variety of polarization colours (first-order to high second-order) depending on their orientation. (*b*) Thin section between crossed polars of a rock containing a large pyroxene crystal, intergrown with other phases marginally. The edges of the crystal are wedge-like, and therefore thinner than the main body. The first-order white to orange colours make a prominent fringe on the right, grading inwards to sensitive tint and then to blue. The main body of the crystal is thus determined as second-order blue. (*c*) A similar section to that in (*a*) (centre of photograph) but here the second-order blue fringe is narrow and is succeeded by a second-order yellow fringe. Hence the main body of the crystal must be showing second-order pink.

marking the first/second-order change is particularly easy to spot because of its generally dark colour. The method is also usable when the crystal grain has a sloping contact with a different crystal, and is especially easy when the latter has significantly lower birefringence. In this case, there are effectively two superimposed wedges (leading to some interesting addition or subtraction effects on R), but counting the fringes in ascending order will lead correctly to the identification of the polarization colour of the high-birefringence grain.

1.6.4.9. *Fast and slow vibration directions*

Before discussing other methods of identifying polarization colours, it is necessary to explain the use of the sensitive-tint plate and the quartz wedge. Both devices consist of a crystal mounted in an elongated holder that can be inserted into a slot in the microscope tube set at 45° to the vibration directions of the polarizer and analyser. The vibration directions of the plates themselves are normally oriented so that the slow ray vibrates NE–SW and the fast ray NW–SE.

The sensitive-tint (or 1λ) plate is made from a cleavage sheet of the white mica, muscovite, and has a thickness such that $R = 560$ nm. To determine fast and slow directions in an unknown specimen, the crystal grain is set to an extinction position and then rotated 45° in either direction. Thus its own vibration directions lie in diagonal positions, and when the tint plate is inserted, the vibration directions of plate and grain are parallel to each other. There are two possible cases depending whether the fast and slow directions coincide or not, *i.e.* slow vibration direction of plate parallel to the slow direction of the crystal (and fast parallel to fast) or slow direction of plate parallel to the fast direction of the crystal.

In the first case, the relative retardation is increased by 560 nm and the observed polarization colour jumps up the scale by one complete order as the plate is inserted. Thus, for example, first-order white ($R = 230$ nm) changes to second-order yellow/green ($R = 790$ nm), second-order blue changes to third-order blue *etc.* When this effect is seen, it shows that the slow direction of the crystal lies NE–SW.

In the converse case, the observed polarization colour also changes, and, if the original colour is at least as high as second-order, will move down the scale by one complete order, *e.g.* second-order orange ($R = 950$ nm) changes to first-order yellow/orange ($R = 390$ nm). If the original colour is, however, within the first order (*i.e.* $R < 560$ nm), the new colour is still a consequence of subtracting 580 nm from R, but it is the absolute value of the new R (not the sign) which is relevant. For example, if the original colour is a first-order grey ($R = 100$ nm), the new colour corresponds to $R = 460$ nm, *i.e.* first-order orange. As a rapid mental aid, it is useful to think of the original colour falling to the bottom of the scale ($R = 0$) and then 'bouncing' back up until a change of one order has been reached, *e.g.* a first-order white, in the middle of the first order, hardly changes (half an order down followed by half an order up); first-order red changes to first-order grey (a fall of 90% of an order, followed by a rise of 10%).

If there is any doubt about the identification of the new colour, the crystal should be rotated through 90° and the second new colour examined. A comparison of the two options available, before and after rotation, rarely leaves any doubt about which is the higher colour (*i.e.* the slow-parallel-to-slow case). In all cases, whether or not the original colour is in the first order, one of the two new colours is higher than the other.

The sensitive-tint plate is so-called because it allows investigation of crystals showing very low birefringence (*e.g.* dark greys with $R \approx 50$ nm or less). In the parallel position, the new colour will lie just on the blue side of sensitive tint, and in the crossed position, just on the red side. These two colours are very easy to distinguish even though they represent only a small change in R.

From the above, it should be clear what an important aid the sensitive-tint plate can be in the actual identification of an unknown polarization colour, whether it be the body colour of the crystal or something observed in a set of grain-margin fringes. There are always two other colours that can be generated using the plate, and their relationship to the original colour is known in terms of R change, so that there are altogether three colours providing information.

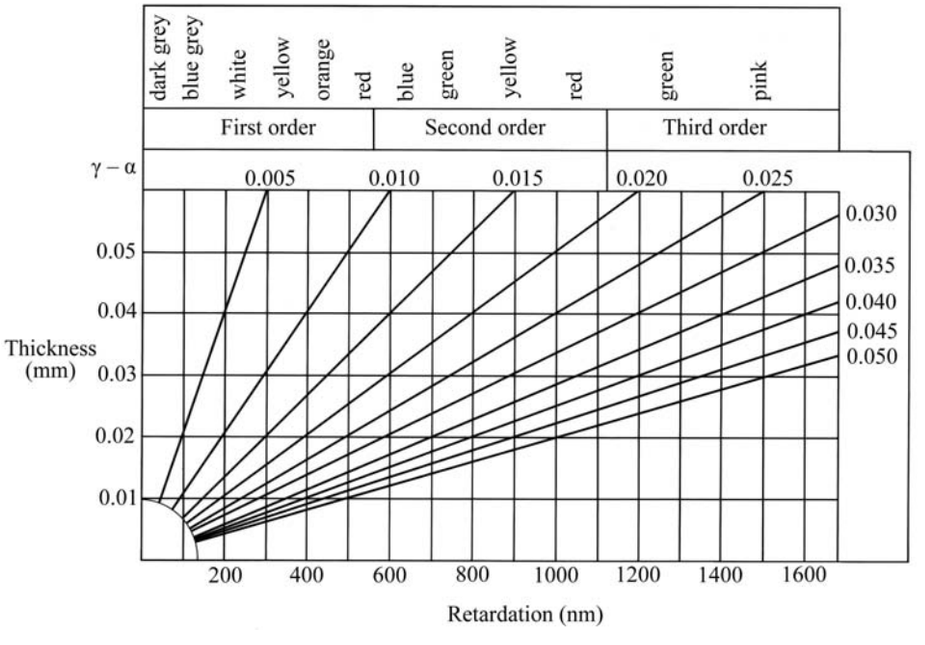

Fig. 1.6.4.6. Polarization colours *versus* thickness. The lines radiating from the origin are of equal birefringence (numerical values are given at the top and the right-hand side of the figure). The diagram may be used to determine thickness if birefringence is known, or birefringence if thickness is known. For example, the diagonal line for birefringence = 0.009 (*e.g.* quartz) intersects the standard thin-section thickness (0.03 mm) on first-order white. This is the polarization colour shown by quartz in a standard thin section.

The *quartz wedge* (Fig. 1.6.4.6) is an elongated wedge-shaped plate of progressively increasing thickness, usually cut parallel to the c axis so that the slow vibration direction is parallel to the length of the wedge. In this form it is inserted into a NE–SW slot so that the slow direction has this orientation. Some microscopes are, however, fitted with a NW–SE slot, and are provided with wedges (and sensitive-tint plates) that are 'length fast' rather than 'length slow'. The optical effects are of course the same in both cases, but it is always a good idea to examine an accessory plate for its vibration directions (marked by the manufacturer) to be on the safe side.

The wedge varies in thickness from almost zero to about 0.2 mm, and typically shows a range of polarization colours from dark first-order grey up to the fourth order or so, as it is progressively inserted into the slot. The wedge can thus be used to change the polarization colour of an observed crystal by any desired amount of R within the available range (roughly 0–2500 nm). By using the two vibration directions of the crystal, these changes can be made additive or subtractive at will. In its simplest possible

application, the crystal is set so that slow is against fast and the wedge is inserted until the crystal shows as close to zero birefringence as possible, *i.e.* the relative retardations of the wedge and the crystal are equal and opposite (this is called *compensation*). Next, the specimen is removed, the colour shown by the wedge noted, and the wedge is slowly pulled out, counting the orders as they go past. This is an accurate and simple alternative method of determining polarization colours.

The accessory plates are useful in identifying the order of polarization colours, but their most frequent application is in determining which of the vibration directions shown by a crystal is fast and which is slow. For example, in a specimen of a biaxial crystal lying with the optic axial plane in the plane of the slide, the slow ray represents γ and the fast ray α. To determine which is which, the vibration directions are set in the 45° position and the tint plate is inserted. If the polarization colour goes up by an order, then the slow direction of the plate is parallel to the slow direction of the crystal. Conversely, if the colour goes down by an order, or goes up by less than a complete order (when the original $R < 560$ nm), fast in the crystal is parallel to slow in the plate.

1.6.4.10. *Other methods of measuring birefringence*

While the use of compensating plates is convenient, more precise techniques have been developed for the measurement of linear birefringence, both in an absolute and in a relative sense. The main methods of making absolute measurements use commercially available compensators mounted on a microscope. The main types are used with a polarizing microscope with crossed polars:

(i) *Babinet compensator*: This is mounted instead of the eyepiece of the microscope, and uses two quartz wedges sliding in opposite directions to each other. The wedges are so designed that when they fully overlap, but without a birefringent specimen in the microscope, a black compensation band is seen in the centre of the field of view. Then when the specimen is placed on the microscope stage in one of the two possible 45° positions, the compensation band is shifted. When in the correct 45° position, as found by trial, the lower wedge is then screwed out to recentre the compensation band, and the distance moved is read from an internal scale. This distance is calibrated in terms of relative retardation.

(ii) *Berek and Ehringhaus compensators*: These use a rotating birefringent crystal to change their effective retardation in order to compensate against the retardation of the specimen. The Berek compensator uses a calcite plate 0.01 mm thick, whereas the Ehringhaus compensator has compound compensating plates of either quartz or calcite, made of two sections of equal thickness cut parallel to the optic axes and cemented above one another at right angles. The compensator is inserted in the slot used for accessory plates with the specimen in one of the two 45° positions. Then by tilting the compensator plate, the apparent retardations are varied until the combined retardation matches that of the specimen, thus giving rise to the compensation band appearing in the centre of the field of view. The angle of tilt can then be converted to relative rotation by the use of suitable tables provided by the manufacturer.

In order to measure birefringence in a relative sense, the following techniques have been devised. All are capable of phenomenal precision in measuring *changes* in birefringence, in some instances to one part in 10^7.

(i) *Sénarmont compensator*: A $\lambda/4$ plate is inserted above the specimen, with one of its principal vibration directions, say the slow direction, parallel to the vibration direction of the polarizer. The analyser is rotatable with a divided circle so that the angle of rotation can be measured. It can be shown that the phase shift of the light δ is given in terms of the angle θ through which the analyser is turned to achieve extinction by

$$\delta = \frac{2\pi}{\lambda}\Delta nz = 2\theta.$$

Thus if the birefringence, or more correctly the relative retardation, of the specimen is changed, say by altering the temperature, one can follow the change simply by monitoring the angle θ. This can be done either manually, or electronically using a phase meter attached to a photomultiplier to measure the intensity as a function of the angle of the analyser, which is rotated at some frequency by a motor.

(ii) *Intensity between crossed polars*: In this case the specimen is placed in the 45° position between crossed polars and the intensity of the light through the system is measured by a photomultiplier and presented typically on a recorder. On changing the retardation of the specimen, say by heating, this intensity changes according to

$$I = I_o \sin^2 \delta/2.$$

Thus on heating a set of $\sin^2$ fringes is drawn out, and by counting the fringes exact measurements of δ can be made. This technique is of great sensitivity, but suffers from the fact that the specimen must be maintained throughout in the 45° position.

(iii) *Rotating analyser*: In this system (Wood & Glazer, 1980), a $\lambda/4$ plate is inserted below the substage but above the polarizer in order to produce circularly polarized light. On passing through a birefringent crystal specimen, this is generally converted to elliptical polarization. This then passes through a Polaroid analyser set to rotate about the axis of the light at a predetermined frequency ω. The resulting intensity is then given by

$$I = (I_o/2)[1 + \sin(2\omega t - 2\varphi)\sin\delta],$$

where φ is the angle between the analyser at any time and an allowed vibration direction of the specimen. Thus by measuring the light intensity with a photomultiplier and then by using, say, phase-sensitive detection to examine the signal at 2ω, a plot of $\sin\delta$ can be made as the specimen's retardation is changed. The fact that circularly polarized light is incident on the specimen means that it is not necessary to align the specimen to any particular angle. Recently, a new type of optical microscope (Glazer *et al.*, 1996) has been developed using this principle, in which false colour images representing I_o, φ and $|\sin\delta|$ can be formed (Fig. 1.6.4.7).

1.6.4.11. *Interference figures*

Interference figures provide one of the most powerful tools for obtaining information about a crystal. The simplest applications allow the division of crystals into uniaxial and biaxial classes, hence constraining the crystal system. Within these classes, crystals are easily divided into the subclasses of positive and negative. More advanced techniques enable the orientation of the indicatrix relative to crystallographic features to be fully established.

Interference figures are obtained when the microscope is used in its *conoscopic* configuration. This means that light is made to pass through the specimen in as wide a range of directions as possible. A powerful substage condenser is inserted to produce a wide cone of incident light and the substage diaphragm is set wide open. A diffusing screen makes a good substitute for the condenser, as it also produces light with a variety of ray directions. However, some brightness is inevitably lost. In either case, a high-power objective with a large numerical aperture is used to collect the light above the specimen, and the polarizer and analyser are crossed.

The distinction between conoscopic and orthoscopic (parallel-light) applications of the microscope is important. For observations of birefringence, the orthoscopic arrangement is required so that optical path lengths through the crystal are constant. The

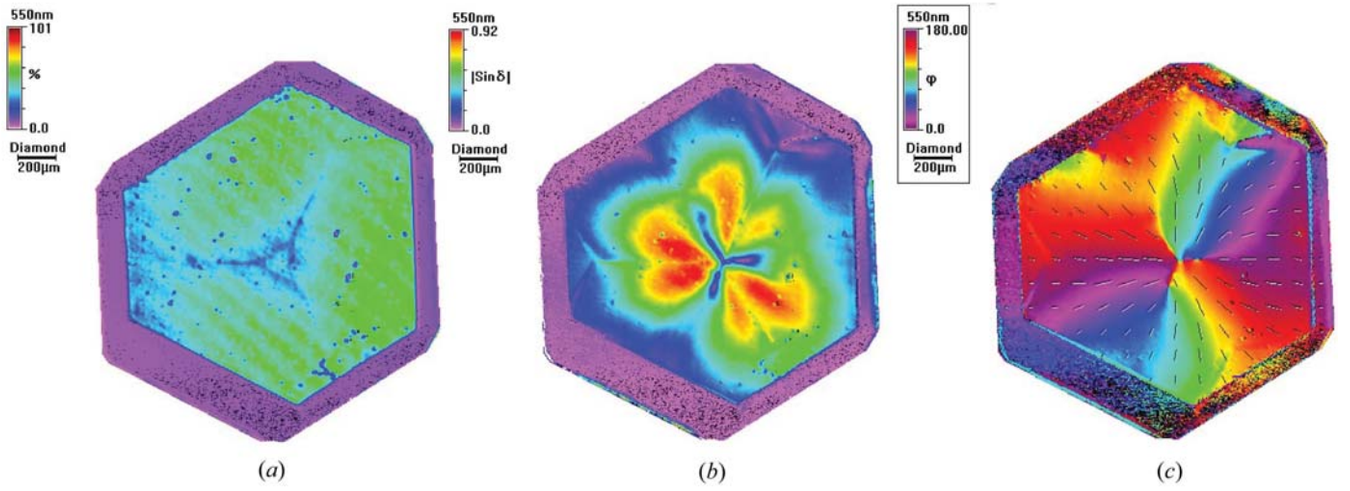

Fig. 1.6.4.7. Three birefringence images of industrial diamond viewed along [111] taken with the rotating analyser system. (*a*) I_0; (*b*) $|\sin\delta|$; (*c*) orientation φ of slow axis with respect to horizontal.

images observed in plane-polarized light rely on scattering from point sources within the specimen, and do not depend strictly on whether the configuration is conoscopic or orthoscopic. Nevertheless, relief and the Becke line are much more clearly observable in orthoscopic use.

The principle of conoscopic use is quite different. Here, the image is formed in the *back focal plane* of the objective. Any group of parallel rays passing through the specimen is brought to a focus in this plane, at a specific point depending on the direction of transmission. Hence every point in the image corresponds to a different transmission direction (see Fig. 1.6.4.8). Moreover, the visible effects are entirely caused by interference, and there is no image of the details of the specimen itself. That image is of course also present, towards the top of the tube at or near the cross wires, but the two are not simultaneously visible. The conoscopic image may be viewed simply by removing the eyepiece and looking down the tube, where it appears as a small but bright circle. More commonly however, the Bertrand lens is inserted in the tube, which has the effect of transferring the conoscopic image from the back focal plane of the objective to the front focal plane of the eyepiece, where it coincides with the cross wires and may be examined as usual.

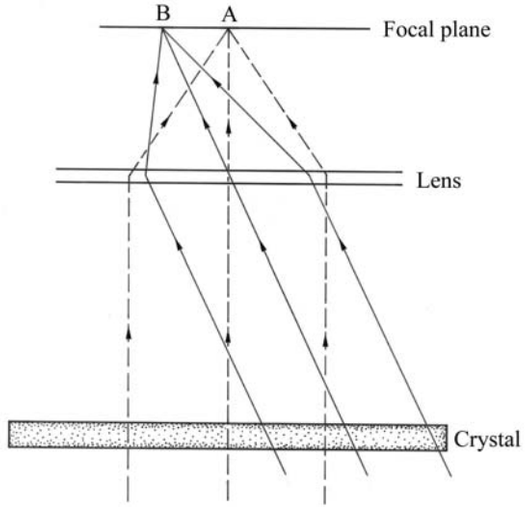

Fig. 1.6.4.8. Formation of the interference figure. The microscope axis lies vertically in the plane of the paper. A bundle of rays travelling through the crystal parallel to the microscope axis (dashed lines) is brought to a focus at A in the back focal plane of the objective. This is the centre of the interference figure. A bundle of oblique rays (solid lines) is brought to a focus at B, towards the edge of the figure.

It is useful to think of the conoscopic image as analogous to the gnomonic projection as used in crystallography. The geometrical principles are the same, as each direction through the crystal is projected directly through the centre of the lens into the back focal plane.

1.6.4.12. *Uniaxial figures*

To understand the formation of an interference figure, consider a simple example, a specimen of calcite cut at right angles to the *c* crystallographic axis. Calcite is uniaxial negative, with the optic axis parallel to **c**. The rays that have passed most obliquely through the specimen are focused around the edge of the figure, while the centre is occupied by rays that have travelled parallel to the optic axis (see Fig. 1.6.4.8). The birefringence within the image clearly must increase from nil in the centre to some higher value at the edges, because the rays here have had longer path lengths through the crystal. Furthermore, the image must have radial symmetry, so that the first most obvious feature of the figure is a series of coloured rings, corresponding in outward sequence to the successive orders. The number of rings visible will of course depend on the thickness of the sample, and when birefringence is low enough no rings will be obvious because all colours lie well within the first order (Figs. 1.6.4.9*a* and *b*). Fig. 1.6.4.10(*a*) illustrates, by reference to the indicatrix, the way in which the vibration directions of the *o* and *e* rays are disposed. Fig. 1.6.4.10(*b*) shows the disposition of vibration directions in the figure. Note that *o* rays always vibrate tangentially and *e* rays radially. The *o*-ray vibration directions lie in the plane of the figure, but *e*-ray vibration directions become progressively more inclined to the plane of the figure towards the edge.

The shaded cross on the figure illustrates the position of dark 'brushes' known as *isogyres* (Fig. 1.6.4.10*b*). These develop wherever vibration directions lie N–S or E–W, hence corresponding to the vibration directions of the analyser and polarizer. As the stage is rotated, as long as the optic axis is truly parallel to the microscope axis, the figure will not change. This is an example of a centred uniaxial optic axis figure, and such a figure identifies the crystal as belonging to the tetragonal, trigonal or hexagonal systems (see Fig. 1.6.4.11*a*).

From the point of crystal identification, one can also determine whether the figure coincides with the uniaxial positive ($n_e > n_o$) or uniaxial negative ($n_e < n_o$) cases. Inserting the sensitive-tint plate will move the coloured ring up or down the birefringence scale by a complete order. Fig. 1.6.4.11(*c*) shows the centred optic axis figure for calcite, which is optically negative. The insertion of a tint plate with its slow vibration direction lying NE–SW lowers the colours in the NE and SW quadrants of the figure, and raises

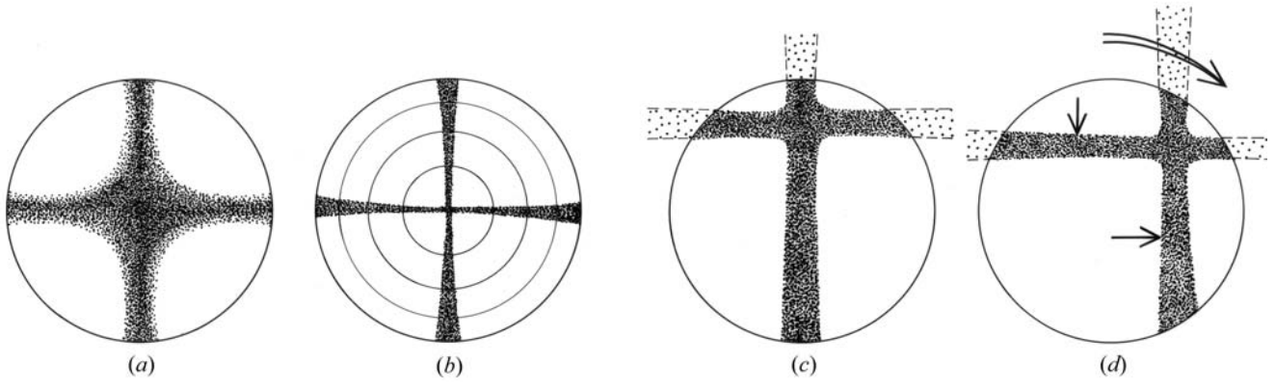

Fig. 1.6.4.9. (*a*) Centred uniaxial optic axis figure of a crystal with low birefringence. The isogyres are diffuse and the polarization colours in the quadrants are likely to be first-order grey. (*b*) As above, but for a crystal with high birefringence. The isogyres are narrower, and circular rings of polarization colours are seen, progressing outwards from first order to higher orders. (*c*) Off-centre uniaxial optic axis figure in the straight position (extinction position of crystal). (*d*) The same rotated to 45°. The curved arrow shows the rotation of the figure as the stage is turned clockwise. Arrows inside the field of view show directions of motions of isogyres. If the optic axis lies outside the field of view, such figures are difficult to interpret and may easily be confused with an off-centre biaxial optic axis figure when $2V$ is small to moderate.

those in the other quadrants (Fig. 1.6.4.11*b*). The simplest general rule is to look at the dark first-order grey in the original figure, lying immediately adjacent to the optic axis, *i.e.* the centre of the cross formed by the isogyres (Figs. 1.6.4.11*b* and *c*). If the crystal is optically negative, this colour changes to first-order yellow in the NE quadrant, if positive to blue. When the crystal has low birefringence, these colours may occupy the whole quadrant.

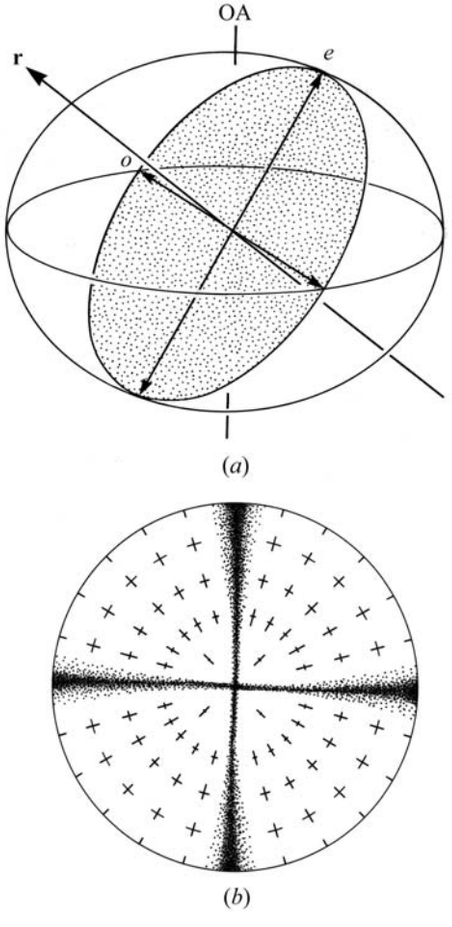

Fig. 1.6.4.10. (*a*) Vibration directions of an oblique ray passing through calcite, viewed relative to the indicatrix. OA is the optic axis, normal to the circular cross section of indicatrix, **r** is the ray direction, *e* and *o* are, respectively, the vibration directions of the extraordinary and ordinary rays in the plane of the elliptical cross section of the indicatrix normal to **r**. (*b*) Vibration directions as seen in the figure. The tangential set represents the *o* rays, the radial set represents *e* rays. The isogyres are also shown.

An *off-centre* uniaxial optic axis figure is obtained when the optic axis is inclined to the microscope axis by an amount which is small enough for it still to be visible within the figure (roughly within 25° of the microscope axis, using a normal high-power objective). Such figures show an isogyre cross with attendant rings, but the centre of the cross does not lie in the centre of the figure, and as the stage is rotated the centre of the cross moves round the figure in a circle (Figs. 1.6.4.9*c* and *d*). The isogyres remain NS and EW throughout. If the figure is so off-centre that the centre of the cross is not visible, the behaviour of the figure becomes difficult to interpret, and may easily be confused with some sorts of off-centre biaxial figures (see below). In the extreme case, when the optic axis lies in the plane of the slide, a quite different figure, known as a *flash figure*, is obtained. This is similar to many of the figures obtained from biaxial crystals, and will be considered further below.

1.6.4.13. *Biaxial figures*

(i) *Acute bisectrix figures*: Biaxial figures may be introduced by considering a crystal with a small $2V$ angle, oriented so that the acute bisectrix is parallel to the microscope axis. The conoscopic figure will have much in common with the uniaxial case already discussed (and indeed will become identical as $2V$ tends to zero), and some form of bilateral rather than radial symmetry is to be expected.

Vibration directions within the figure can be deduced by consideration of the *Biot–Fresnel* construction. Given that the form of the indicatrix is known, this is used to determine vibration directions in any orientation required. A general case presented in the form of a stereographic projection is given in Fig. 1.6.4.12(*a*). It is first necessary to know the positions of the optic axes and the position of a ray direction. Two planes are constructed, each containing one optic axis and the ray direction. Two *additional* planes are constructed, each containing the microscope axis and *bisecting* the angles between the first two planes. The plane in which the vibration directions lie is plotted normal to the ray direction, and the two vibration directions in this plane are fixed by the intersections of this plane with the two additional planes. This is also a very powerful construction to use in conjunction with orthoscopic methods. If crystallographic features, *e.g.* traces of cleavage planes, crystallographic axes, twin planes *etc.* (twinning is discussed in Chapter 3.3) are added to the stereogram, it becomes possible to determine the predicted angles between vibration directions and crystallographic features. One of the most fundamental aims of polarizing microscopy is the determination of the complete orientation of the indicatrix relative to crystallographic directions. Familiarity with the Biot–Fresnel construction is a substantial aid.

Returning to the interference figure, a modified version of the Biot–Fresnel construction is illustrated in Fig. 1.6.4.12(*b*). Since the interference figure is analogous to a gnomonic rather than a stereographic projection, the various constructional planes required are straight lines. The vibration directions for the complete figure are given in Fig. 1.6.4.12(*c*).

Considering first the isogyres (brushes), if the optic axial plane lies N–S, as in Fig. 1.6.4.13(*a*), clearly the isogyres form a cross, as in the uniaxial case. There is a small difference, however. Because the vibration directions curve round more rapidly near the optic axial plane, the N–S isogyre is sharper than the E–W, which is relatively broadened and less dark.

If the slide is rotated so that the optic axial plane lies NE–SW, inspection of the vibration directions in Fig. 1.6.4.13(*b*) shows that the isogyres must part in the direction shown. Rotation of the stage through a full 180° will thus show two positions at which the brushes cross – once when the optic axial plane lies N–S, the other when it lies E–W – and two positions of maximum separation of the isogyres – when the optic axial plane lies NE–SW and NW–SE (see Fig. 1.6.4.14*a*). The position of the broader, more diffuse, brush will alternate. The amount by which the two isogyres are separated in the 45° position depends on the size of $2V$. Since the field of view is usually about 60°, when $2V$ is 60° the isogyres will retreat right to the edge of the field of view in the 45° position, and then come back as rotation continues. When $2V > 60°$, the brushes will entirely leave the field of view for part of the rotation (Fig. 1.6.4.14*c*). Approximate estimates of $2V$ can be made on this basis.

As in the uniaxial case, coloured fringes are also part of the figure, and are most obvious when birefringence is high (Fig. 1.6.4.14*a* and Fig. 1.6.4.15*a*). The outermost fringes have an elliptical form, but towards the centre of the figure they are distorted into a dumbbell-like or figure-of-eight form. This arises

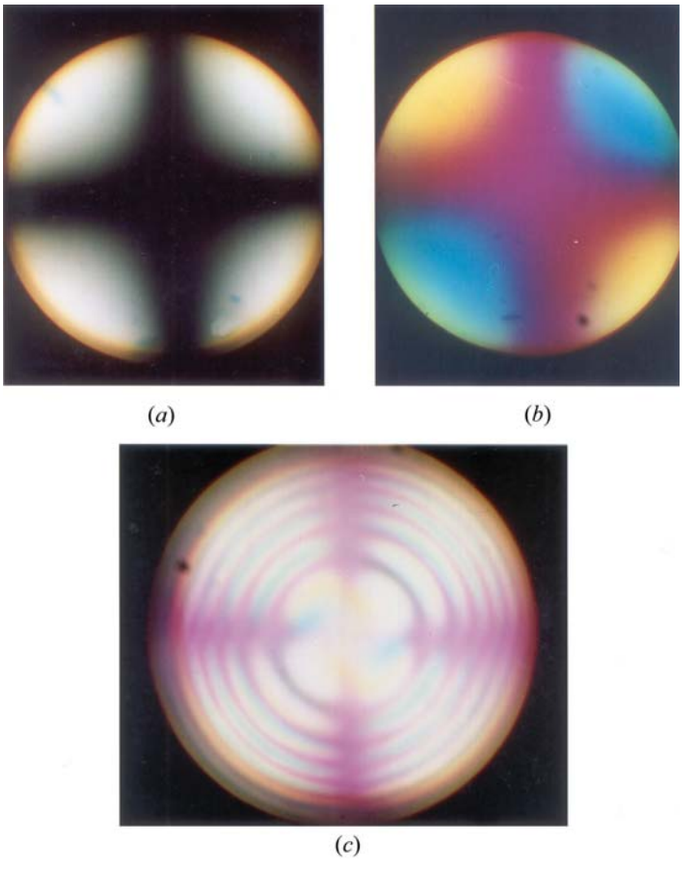

Fig. 1.6.4.11. (*a*) Centred optic axis figure of quartz (uniaxial). The birefringence is low, resulting in a diffuse cross and quadrant colours in the lower half of the first order. (*b*) The same figure with the sensitive-tint plate inserted (slow vibration direction NE–SW). The isogyres take on the sensitive-tint colour. Compensation takes place in the NE and SW quadrants (slow directions of crystal and plate parallel to each other) resulting in second-order blue, that is, one whole order above the original. In the other quadrants, the colours also apparently rise, but are restricted to yellow (high first-order). Thus the crystal is optically positive, that is, *e* rays (radial) are slow and *o* rays (tangential) are fast. (*c*) Centred optic axis figure of calcite with sensitive-tint plate (slow direction lying NE–SW) inserted. The birefringence is very high so there are many coloured rings. In the top right quadrant, the colour immediately adjacent to the cross is first-order yellow, whereas in the top left it is second-order blue. Calcite is hence optically negative. It can be observed that all the coloured rings in the top right and bottom left quadrants are an order lower than their counterparts in the top left and bottom right.

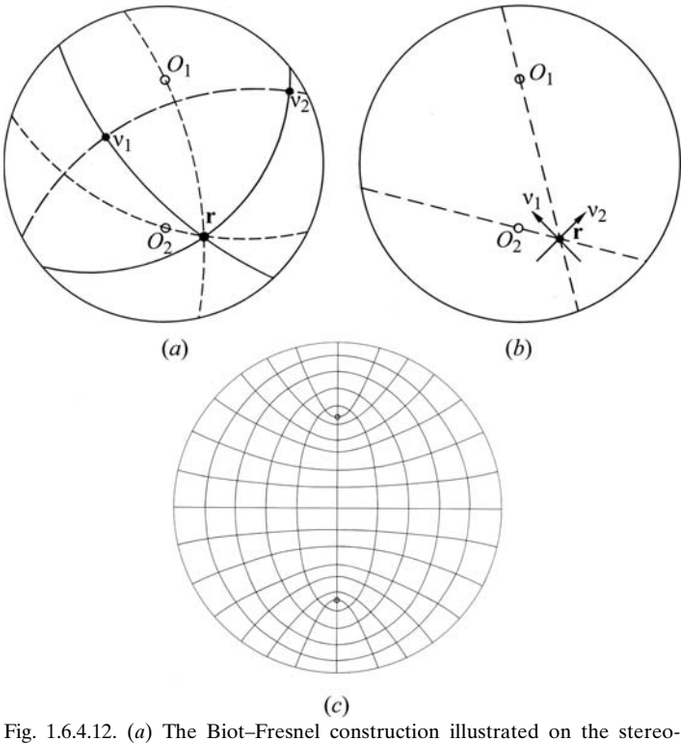

Fig. 1.6.4.12. (*a*) The Biot–Fresnel construction illustrated on the stereographic projection. (*b*) Method of determining vibration directions in a biaxial acute bisectrix figure using the Biot–Fresnel construction and a gnomonic projection. (*c*) Complete vibration directions of a figure similar to the above. As noted in the text, the directions shown are components resolved into the plane of the figure, and the true vibration directions are in general somewhat inclined.

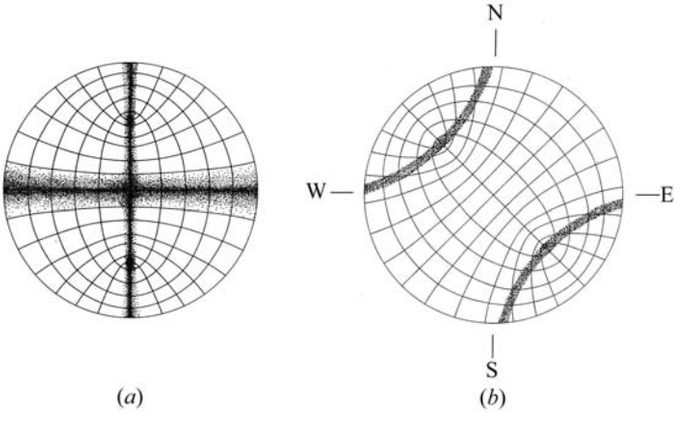

Fig. 1.6.4.13. (*a*) Illustration of the formation of crossed isogyres when the optic axial plane of a biaxial figure lies N–S. The shaded lines illustrate the zones in which vibration directions are N–S and E–W, leading to the formation of the isogyres. Along the E–W line, the zone across which vibration directions depart little from N–S and E–W is broad, hence this isogyre is wider than the N–S isogyre. (*b*) Illustration of the formation of separated curved isogyres when the same crystal is in the 45° position (optic axial plane NE–SW).

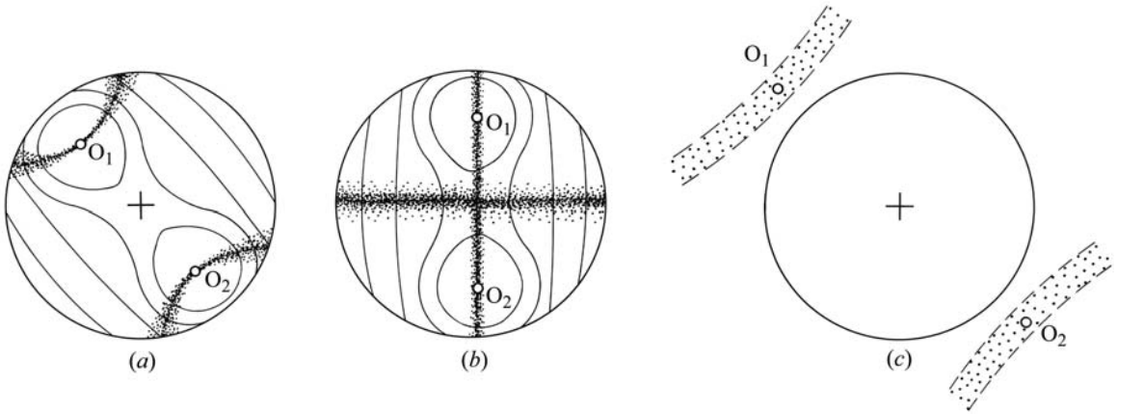

Fig. 1.6.4.14. (*a*) Drawing of biaxial optic axis figures set in the 45° position with the optic axial plane set NW–SE. $2V$, represented by the angle O_1–O_2, is about 40° (*cf.* total field of view of *ca* 60°). The distribution of coloured fringes is represented, with near-circular areas of first-order colours around the optic axes, progressing outwards to higher orders (see also Fig. 1.6.4.15*a*). (*b*) The same figure in the straight position (optic axial plane N–S). Note that the isogyre along the optic axial plane is sharper than the E–W isogyre. (*c*) Representation of a biaxial figure in the 45° position when $2V > 60°$. The isogyres leave the field completely.

because the areas of minimum birefringence must lie adjacent to the optic axes, and birefringence, although generally increasing outwards, must also increase towards a point midway between the optic axes. This effect is slight when birefringence is low, but is prominent when birefringence is high, in which case each optic axis is surrounded by its own set of almost-circular fringes, set within the general elliptical array.

Optic sign can be determined from the acute bisectrix biaxial figure in a way analogous to the uniaxial case. The stage is rotated to the 45° position, *i.e.* with maximum separation of the isogyres, and the analogues of the uniaxial quadrants are identified. The difference here is that in one of the 45° positions the NE and SW quadrants join through the space between the optic axes, and in the other the NW and SE quadrants are connected. The sensitive-tint plate is employed just as in the uniaxial case, and the same rules apply to change of colour (Fig. 1.6.4.15*a* and *b*). For example, suppose that the stage is turned so that the NE and SW quadrants are separated from each other. Optically positive crystals show second-order blue close to the isogyre within the quadrant (on the concave side of the isogyre), while first-order yellow appears on the convex side, which is part of the combined NW and SE quadrants. Optically negative crystals show the reverse.

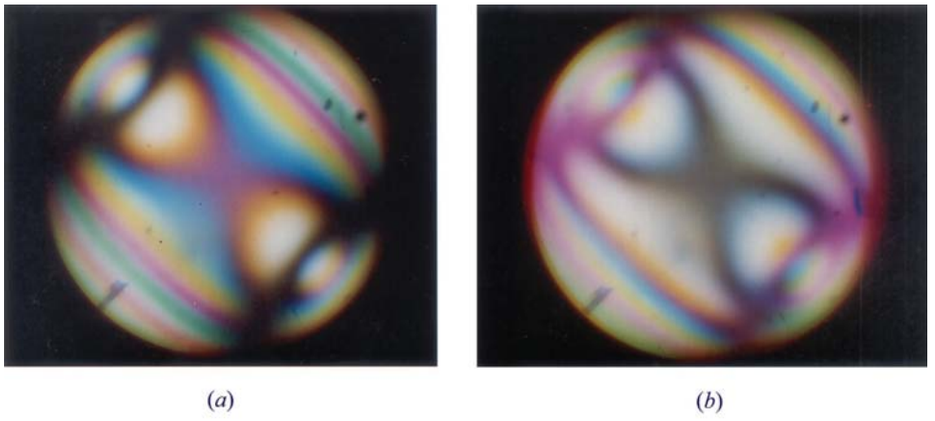

Fig. 1.6.4.15. (*a*) Acute bisectrix figure of a biaxial crystal with $2V \simeq 40°$. The optic axial plane is oriented NW–SE. First-order colours are confined to the two circular 'eyes' or melatopes around the optic axes, with sensitive tint itself making a figure-of-eight shape ('dumbbell'). At the edge of the figure in the NE and SW directions the coloured fringes reach third-order pink. (*b*) The same figure with the sensitive-tint plate inserted (slow direction NE–SW). The isogyres have taken on the sensitive-tint colour. Between the optic axes (*e.g.* the centre of the figure), the original sensitive-tint dumbbell has become black, and to the NW and SE of the centre all the fringes have dropped by one order. Conversely, in the extreme NW and SE directions all fringes have gained an order. The little patches of yellow lying just inside the optic axes, and the accompanying blue patches just outside, indicate by analogy with the uniaxial figure that the crystal is optically negative.

Slightly off-centre acute bisectrix figures are easy to interpret if $2V$ is low, but as the degree of off-centring increases, and as $2V$ increases, it is obvious that interpretational difficulties will rapidly increase, and recourse must be made to the optic axis figure.

(ii) *Optic axis figures*: Although the acute bisectrix figure forms the most convenient introduction to the subject, it is in practice quite difficult to find a suitable section without trial and error. In monoclinic and triclinic crystals, for example, the acute bisectrix section is not in general identifiable by reference to crystallographic features (cleavage, faces *etc.*), nor by any special optical properties observable under orthoscopic conditions. As in the uniaxial case, however, the optic axis section is identifiable by its low-to-nil birefringence. The optic axis figure is the workhorse of the microscopist.

The essential feature of this figure is that, as the stage is rotated, one of the optic axes is positioned permanently in the centre of the field of view, while the other rotates around it. One of the isogyres is always visible. When $2V$ is small, on rotation of the stage the figure simply looks like a wobbly version of the acute bisectrix figure. Both isogyres are visible, and determination of optic sign, using the sensitive-tint plate, is as described above.

As $2V$ increases, however, the second isogyre leaves the field during part of the rotation, and the point where the isogyres cross, when the optic axial plane lies N–S or E–W, moves towards the edge of the field of view. Eventually, with further increase of $2V$, the second isogyre does not enter the field of view at all, and the figure consists of a single brush rotating about the optic axis. The brush changes from straight, when it lies N–S or E–W, to curved, when the crystal is in the 45° position, and the degree of curvature decreases with rising $2V$. When $2V = 90°$, the brush remains straight in all positions. With experience, the maximum curvature of the isogyre can be used for rough estimation of $2V$.

Optic sign is readily determined from any sort of optic axis figure by setting the crystal in the 45° position and using the curvature of the isogyre to identify the various 'quadrants' as described above. This of course is not possible when

$2V = 90°$, and such crystals are described as optically neutral.

A further piece of useful information is derivable from optic axis (and acute bisectrix) figures, *i.e.* the direction of the optic axial plane, that is, the line joining the two optic axes. Even if the second isogyre is never visible, the position of the second optic axis, outside the field of view, is easily judged. By reverting to orthoscopic observation without moving the specimen, it is easy to see how the optic axial plane relates to crystallographic features such as faces, cleavages or twin planes.

(iii) *Other biaxial figures*: Several special figures are occasionally useful, and their behaviour is readily explained by comparison with the acute bisectrix figure. The obtuse bisectrix figure behaves like the acute bisectrix figure, but as if $2V$ were very large. The isogyres form a diffuse cross in the centre of the field, and then, on rotation, rapidly depart from the field, either *via* the NE and SW quadrants or *via* the NW and SE. As rotation approaches 90°, they re-enter the field of view from the other direction. When $2V$ approaches 90°, there is of course very little difference between the acute and obtuse bisectrix figures, and to determine which is which it is necessary to measure the speed at which isogyres leave the field of view during rotation (for a given rotation the obtuse bisectrix isogyres move further).

The optic normal figure (often known as a *flash figure* because of the extreme speed of isogyre movement) is formed when the optic axial plane lies in the plane of the slide. Its behaviour on rotation of the stage is an extremely rapidly moving version of the obtuse bisectrix figure. The isogyres are very broad and diffuse, and when the cross is formed there is little more than a momentary darkening of the whole field of view. The brushes vanish completely from the field with only a very small rotation from this position. Often it requires careful inspection even to be certain that the cross splits into two brushes that vanish diagonally from the field.

The optic normal figure is useful in orientation studies and, as mentioned above, grain mounts of orthorhombic crystals may naturally give rise to suitably oriented crystals. In thin sections, the figure is useful to confirm that grains apparently showing maximum birefringence do in fact lie with their optic axial planes normal to the microscope axis. When only a small number of grains are available, this check is important.

In the most general sense, this exercise illustrates that all figures are variations on a single theme, in which the vibration direction diagram of Fig. 1.6.4.12(*c*) can be thought of as being viewed from different distances (delimiting the size of the area viewed) and different directions (*i.e.* where the centre of the field of view is, relative to the centre of the diagram). For, example, the figure shown represents a centred uniaxial optic axis figure if viewed from infinite distance in a direction corresponding to the centre of the diagram. On the other hand, if viewed from close up in the same direction (so that the field of view is thought of as a rather small circle in the middle of the diagram), the figure becomes analogous to the acute bisectrix figure of a crystal with a large $2V$, the obtuse bisectrix figure, or even the uniaxial flash figure (but see below), with increasing distance of the viewpoint. Off-centre figures can be equally well explained by placing the viewpoint non-centrally.

Only the uniaxial flash figure and the biaxial optic normal figure seem, at first sight, to defy exact interpretation, because the optic axes, lying in the plane of the figure, seem to require to be plotted at infinity in the plane of the paper. This then requires that the map of the vibration directions consists of two linear sets at a right angle to each other. No explanation of the rapid separation of the diffuse isogyres accompanying a small rotation from the extinction position is forthcoming. Rather, a simple extinction of the whole field is predicted at every 90°.

In fact, the vibration directions seen in such figures still retain the 'barrel-shaped' configuration seen in Fig. 1.6.4.12(*c*), though degrees of curvature can be very small. This arises because the true vibration directions of, for example, the *e* rays in the uniaxial case, do not lie in the plane of the figure (except at the centre). A curved surface is required for the true description of the vibration directions. We have up to this point regarded the diagram as flat, but in fact the vibration directions, as we view them, become distorted into the barrel shape.

1.6.4.14. *Orientation studies*

The full skills of the microscopist are required in the production of an accurate description of the optical orientation of a sample, that is the relationship of the indicatrix to the crystallographic axes.

It is best to start by determining the crystal system. Completely isotropic crystals are cubic, uniaxial crystals are tetragonal, trigonal or hexagonal, while biaxial crystals are orthorhombic, monoclinic or triclinic. Crystallographic features such as edges, faces, crystal outlines, shapes, cleavages and twin planes give the additional information required to subdivide the uniaxial and biaxial classes.

In uniaxial cases, a grain giving a centred optic axis figure is required. If the crystals look square, or have cleavages and/or twin planes intersecting at right angles, then the system is most likely to be tetragonal. Features disposed as equilateral triangles indicate triclinic, and hexagonal arrangements may indicate triclinic or hexagonal. The cases are often impossible to distinguish.

Orthorhombic crystals are usually fairly easy to identify because, although biaxial, they still show parallelism between many optical and crystallographic properties. For example, vibration directions commonly lie parallel to the traces of cleavage planes or crystal outlines (so-called *straight extinction*). Alternatively, vibration directions may bisect the angles between such features (*symmetrical extinction*). Furthermore, crystals with obviously special orientations can be identified, *e.g.* a section showing two sharply defined cleavages (*i.e.* lying at right angles to the plane of the slide) perhaps at right angles to each other, or producing a diamond pattern, is obviously cut normal to an important crystallographic direction, perhaps containing two of the crystallographic axes. The interference figure of such a section should be examined carefully as it is likely to be a centred version of the acute bisectrix, obtuse bisectrix or flash figure.

Monoclinic crystals are extremely common, and, while biaxial, do not generally show the parallelism of optical and crystallographic features typical of the orthorhombic system. There is no general recipe for success in determining the optical orientation of such crystals, other than systematic observation of crystals in different orientations. The most important observations are the relationships between extinction positions and crystallographic features, and the nature of the interference figures. All monoclinic crystals have one plane that, if at right angles to the slide, shows symmetrical or straight extinction. This plane is observed when the twofold symmetry axis lies in the plane of the slide. In crystals that show two cleavages, their intersection is also likely to mark a crystallographic axis. From consideration of such features it is often possible to identify a crucial special section, that lying perpendicular to the twofold axis. This is an important section, because two crystallographic axes now lie in the plane of the slide and their directions may be indicated by cleavage traces, crystal edges *etc.* Determination of the angles between vibration directions and supposed crystallographic axis directions then gives the important angle (*e.g.* n_γ, **c**) which expresses the tilt of the indicatrix within the plane normal to the twofold axis.

If everything fails, and no relationship can be found between crystallographic and optical directions, the crystal is probably triclinic, and it is not possible to say very much about its orientation using the flat-stage microscope. Recourse must then be had

to the *universal stage*, a device that allows rotation of the slide in three dimensions. This is rarely done these days.

Orientation studies are completed by assigning specific axes of the indicatrix to specific crystallographic axes. The identification of the principal axes of the indicatrix is easy. For example, in uniaxial cases, sections showing maximum birefringence contain the unique crystallographic axis, which is parallel to the n_e direction. Knowledge of the optic sign shows which of the two vibration directions coincides with n_e, on the basis of being fast or slow. In biaxial cases, the maximum birefringence section has n_α and n_γ lying in the plane of the slide, and of these n_γ corresponds of course to the slow ray. In biaxial crystals, the identification of the optic axial plane direction in a figure enables immediate identification of the n_β direction, which is normal to it.

1.6.4.15. *Absorption colours*

Many crystalline substances are coloured in transmitted light under the microscope, as a result of the absorption of certain visible-light wave bands. Though there may be much variability between one sample of a substance and another, colour is nevertheless often a great aid in identification.

Absorption, like other optical phenomena, is capable of showing marked anisotropy, the phenomenon known as pleochroism. Pleochroism is usually obvious in both grain mounts and thin sections, because grains change colour when rotated in plane-polarized light. The effect can be subtle (*e.g.* the mineral hypersthene is almost colourless in thin sections but often shows pleochroism from a very faint pink to a very faint green), or very marked (*e.g.* dark brown to colourless or pale yellow in the mineral biotite). The full description of pleochroism involves the assigning of different colours to specific axes of the indicatrix. Uniaxial crystals are *dichroic*, that is, two colours describe the effects. Sections showing centred optic axis figures do not exhibit pleochroism, showing only the pure absorption colours of light vibrating normal to the optic axis (n_o). In biotite for example (which is for practical purposes uniaxial), this colour is usually dark brown. Maximum birefringence sections, or those showing centred flash figures in grain mounts, show maximum pleochroism, one vibration direction exhibiting the n_o absorption already noted, and the other the pure effects of absorption on n_e (in the case of biotite, colourless to pale yellow). Random sections show less pleochroism, and colours that are combinations of the pure end members.

Biaxial crystals can be notably trichroic, and colours are readily assigned by looking at maximum birefringence (flash figure) sections to obtain n_α (fast ray) and n_γ (slow ray) absorptions, and optic axis sections to obtain that for n_β.

The other notable thing about absorption colours is that they can occasionally severely mask polarization colours. Once this is appreciated, the use of the sensitive-tint plate is often sufficient to identify the latter.

1.6.4.16. *Dispersion*

Dispersion, that is to say variation of refractive index depending on wavelength, is a common phenomenon in crystals, and occasionally an important aid in identification. In extreme cases, it results in the production of highly anomalous polarization colours, often browns, blue greys or brownish purples, or bright colours which just look slightly unusual compared with normal second- or third-order colours. Anomalous colours are highly diagnostic of certain substances (*e.g.* the minerals chlorite, zoisite and epidote).

Dispersion also results in a lack of definition of extinction positions, because in biaxial crystals there may effectively be differently oriented indicatrices for different wavelengths. In extreme cases, it may be impossible to locate the extinction position with any accuracy. As an example of a milder case, the very common mineral plagioclase (triclinic) shows subtle, though highly characteristic, features between crossed polars in sections cut approximately normal to the b crystallographic axis. The normal polarization colours seen in between the extinction positions are pure first-order greys and whites, but as a grain is rotated slowly through an extinction position the colours darken and take on a bluish (cold) tinge before going black, and then lighten again with a yellowish (warm) tinge. This is the result of a slight mismatch of the orientations of the indicatrices for long and short wavelengths.

Such dispersion is also often obvious (at least, when looked for) in the interference figures of biaxial crystals. Isogyres become edged with 'cold' (*i.e.* bluish) and 'warm' (tending to red or orange) fringes on opposite sides, indicating that optic axes for different wavelengths have slightly different positions.

Dispersion is a difficult phenomenon to investigate fully with the polarizing microscope. In cubic crystals, it can only be studied systematically by the determination of refractive indices using a number of monochromatic light sources of different wavelengths. Uniaxial crystals can show anomalous polarization colours, but they do not show fringes in interference figures, nor vagueness in extinction position, because the indicatrices for different wavelengths all have the same orientation. Like cubic crystals, however, the dispersion can be investigated by monochromatic light studies of refractive index. Biaxial crystals present the most complex cases. Not only can the shape of the indicatrix vary with wavelength (*i.e.* the relative values of the principal refractive indices), but so can orientation relative to the crystallographic axes. There are even substances known (admittedly with small $2V$) in which the optic axial plane for red light is at right angles to the optic axial plane for violet light. The phenomenon is known as 'crossed axial plane dispersion', a real challenge for the microscopist.

1.6.5. Optical rotation

1.6.5.1. *Introduction*

Optical rotation or gyration, as it is sometimes known, was first recorded by Arago in 1811. Since then, a great deal of work has been done to try to explain this phenomenon, and at the present time it is one of the few physical properties of a crystal that can be successfully understood in terms of the underlying crystal structure (Glazer & Stadnicka, 1986). Lowry (1935) has given a good historical account of the subject.

Optical rotation is the phenomenon observed in some crystals (and in some solutions of, usually, organic compounds) of the rotation of plane-polarized light on passing through the crystal. If the rotation, as seen by the observer, is to the left or counterclockwise it is known as *laevorotation*; if to the right or clockwise it is known as *dextrorotation*. A crystal that shows this effect is sometimes called *optically active* or *gyrotropic*. It is therefore clear that, from a symmetry point of view, optical rotation can only occur in a crystal in which one direction is not equivalent to its opposite, *i.e.* there are no inversion symmetry operations that can change chirality.

One of the earliest theories to explain the origin of optical rotation was given by Fresnel. This was based on the idea that a plane-polarized wave can be equally described by two opposing circularly polarized waves propagating along the same direction. In Fig. 1.6.5.1(*a*), the polarization vector **OA** is simply given by the vector sum of **OB** and **OC**, polarization vectors at some instant of time belonging to a right-circular and a left-circular wave, respectively. Here it is assumed that the light propagates in a direction towards the viewer. If the light now passes through a gyrotropic material, one of the circularly polarized waves will be slowed down with respect to the other (this corresponds to having a small difference in refractive indices for the two waves). Thus on emerging from the crystal, there will be a phase difference between the circular waves, so that on recombining, the resulting

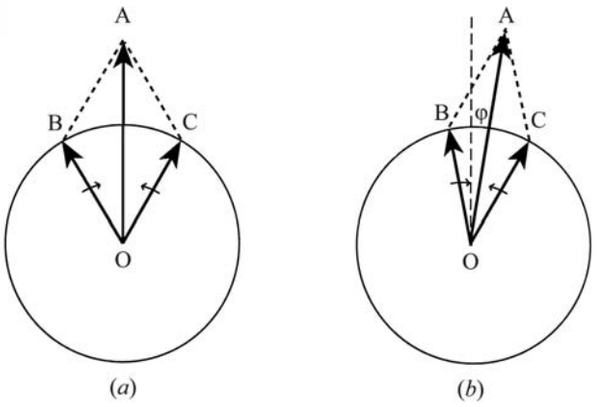

Fig. 1.6.5.1. Fresnel's explanation of optical rotation.

plane of linear polarization **OA** will have rotated through an angle φ. This is shown in Fig. 1.6.5.1(b), where the right-circular (*clockwise*) component travels faster than the left-circular (*anticlockwise*) component. Because of this, in a given time, the electric vector for the right-circular wave, observed in a fixed plane perpendicular to the line of sight, will have rotated through a larger angle clockwise than the electric vector for the left-circular wave will have rotated anticlockwise. The result is a net rotation to the right, *i.e.* dextrorotation, of the vector **OA**. The left and right-circular refractive indices, n_L and n_R, are inversely related to the velocities of the waves, and so Fig. 1.6.5.1(b) corresponds to the case where $n_L > n_R$. Thus this theory shows that a positive value of $n_L - n_R$ defines dextrorotation and that optical rotation is in fact a form of *circular birefringence*.

Fig. 1.6.5.2 illustrates in a more generalized way the nature of the birefringences possible in a crystal. Formally, the refractive index of a medium can be written in terms of real and imaginary components:

$$n = n' + in'', \tag{1.6.5.1}$$

the imaginary component referring to the absorption of the light (the real and imaginary terms are related as usual by the Kramers–Kronig relationship). Similarly, the linear and circular birefringences can also be written in real and imaginary terms:

$$\begin{aligned} \Delta n_{\text{linear}} &= (n_1 - n_2)' + i(n_1 - n_2)'' \\ \Delta n_{\text{circular}} &= (n_L - n_R)' + i(n_L - n_R)''. \end{aligned} \tag{1.6.5.2}$$

The real linear birefringence (a) shows a resonance, changing sign, at a particular wavelength. Its variation with wavelength is known as *birefringent dispersion*. The imaginary component (b) peaks at this wavelength and corresponds to the difference in absorption between linear polarization states. This is called *linear dichroism* (LD) and is determined by quantum-mechanical selection rules resulting from matrix elements of the type $\langle \Psi_1 | \hat{p} | \Psi_0 \rangle$, where $\hat{p}$ is the electric dipole operator. The circular components follow similar behaviour. The real circular birefringence (c) corresponds to the optical rotation and its change with wavelength is known as *optical rotatory dispersion* (ORD). The imaginary circular birefringence (d) corresponds to the difference in absorption of opposite circularly polarized states. This is called *circular dichroism* (CD) and is determined by the matrix elements of the type $\langle \Psi_1 | \hat{\alpha} | \Psi_0 \rangle$, where $\hat{\alpha}$ is the polarizability operator. Since $\hat{\alpha}$ is an even function, whereas $\hat{p}$ is an odd function, the selection rules for LD and CD are different, and each type of spectrum gives different information.

The link between optical rotation and crystal structure has been the subject of a great deal of work from the 18th century to date. Experimental methods for determining absolute chirality (Glazer & Stadnicka, 1989) of crystals only became routine in the late 1940s with the use of the X-ray anomalous dispersion effect,

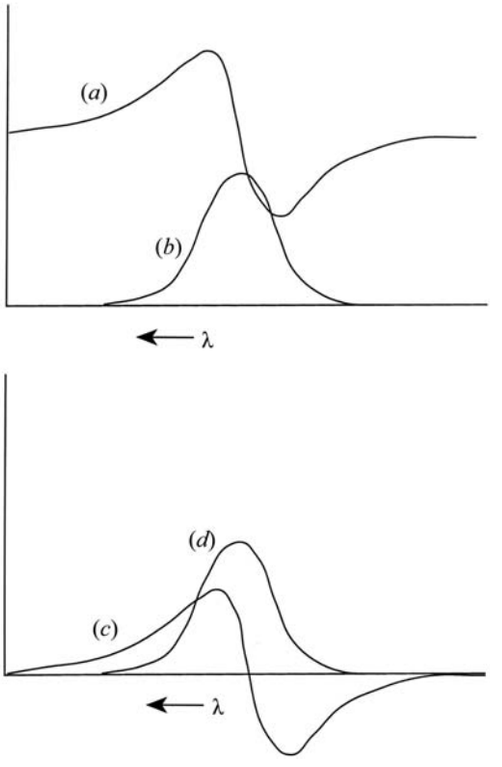

Fig. 1.6.5.2. Real and imaginary birefringence as a function of wavelength: (a) real linear; (b) imaginary linear; (c) real circular; (d) imaginary circular.

which made it possible to determine the absolute sense of the chiral nature of a crystal and then to link this to the sense of optical rotation. However, despite the preponderance of a great many complex theories, until recently, experimental evidence to support these theories has been fragmentary. It was shown by Glazer & Stadnicka (1986) that, at least for inorganic crystals, the problem lay in mistakes in the experiments or publications describing the experiments, rather than in the underlying theories. Once these errors are taken into account, it is possible to find a direct link between the chiral nature of the structure and the optical rotation, which appears to work in almost all cases. It has even been possible to produce a computer program *OPTACT* (Devarajan & Glazer, 1986; Glazer, 2002), using a polarizability theory based on earlier work by Born (1933), that is capable of calculating both the sign and magnitude of the effect with reasonable precision in many cases. *OPTACT* also calculates the refractive indices with good reliability.

1.6.5.2. *The dielectric tensor and spatial dispersion*

The relevant polarization term to consider here is

$$P_i^{\omega} = \omega_0 \chi_{ij\ell} \nabla_{\ell} E_j^{\omega}. \tag{1.6.5.3}$$

The important part of this expression is the use of the field gradient, which implies a variation of the electric field across the unit cell of the crystal rather than the assumption that **E** is everywhere constant. This variation in **E** is known as *spatial dispersion* (Agranovich & Ginzburg, 1984).

Assume propagation of a plane wave given by $\mathbf{E} = \mathbf{E_o} \exp(i\mathbf{k} \cdot \mathbf{r})$ through an optically active crystal. Substituting into the expression for the polarization gives

$$P_i^{\omega} = i\omega_0 \chi_{ij\ell} E_j^{\omega} k_{\ell}. \tag{1.6.5.4}$$

This term can now be treated as a perturbation to the dielectric tensor $\varepsilon_{ij}(\omega)$ to form the *effective* dielectric tensor $\varepsilon_{ij}(\omega, \mathbf{k})$:

$$\varepsilon_{ij}(\omega, \mathbf{k}) = \varepsilon_{ij}(\omega) + i\gamma_{ij\ell} k_{\ell}, \tag{1.6.5.5}$$

where $\gamma_{ij\ell}$ has been written for the susceptibility $\chi_{ij\ell}$ in order to distinguish it from the use of χ elsewhere. Note that this can be expressed more generally as a power-series expansion in the vector $\mathbf{k}$ (Agranovich & Ginzburg, 1984) to allow for a generalization to include all possible spatial dispersion effects:

$$\varepsilon_{ij}(\omega, \mathbf{k}) = \varepsilon_{ij}(\omega) + i\gamma_{ij\ell}(\omega)k_\ell + \alpha_{ij\ell m}(\omega)k_\ell k_m, \tag{1.6.5.6}$$

where the susceptibilities are in general themselves dependent on frequency.

1.6.5.3. *Symmetry of effective dielectric tensor*

To determine the symmetry constraints on the effective dielectric tensor, it should be recognized that the application of a real electric field $\mathbf{E}$ must lead to a real dielectric displacement $\mathbf{D}$. This therefore implies that one can write

$$\varepsilon_{ij}(\omega, \mathbf{k}) = \varepsilon^*_{ij}(-\omega^*, -\mathbf{k}^*)$$

or

$$\varepsilon_{ij}(\omega^*, \mathbf{k}^*) = \varepsilon^*_{ij}(-\omega, -\mathbf{k}). \tag{1.6.5.7}$$

Furthermore, in the absence of any absorptive processes, ε_{ij} must be Hermitian, that is

$$\varepsilon_{ij}(\omega, \mathbf{k}) = \varepsilon_{ji}(\omega, -\mathbf{k}). \tag{1.6.5.8}$$

This is fulfilled by the following symmetry constraints for the leading terms in the effective dielectric tensor:

$$\varepsilon_{ij}(\omega) = \varepsilon_{ji}(\omega); \quad \gamma_{ij\ell}(\omega) = -\gamma_{ji\ell}(\omega); \quad \alpha_{ij\ell m}(\omega) = \alpha_{ji\ell m}(\omega). \tag{1.6.5.9}$$

In a gyrotropic crystal, there must be at least one direction that is not equivalent to its opposite, and so such a crystal cannot have a centre of symmetry. (Only a noncentrosymmetric crystal can be gyrotropic. However, it is true to say that all non-gyrotropic crystals must be centrosymmetric.) Therefore, for a non-gyrotropic crystal,

$$\varepsilon_{ij}(\omega, \mathbf{k}) = \varepsilon_{ij}(\omega, -\mathbf{k}). \tag{1.6.5.10}$$

It follows therefore in such a case that

$$\gamma_{ij\ell}(\omega) = 0. \tag{1.6.5.11}$$

It is obvious then that the susceptibility $\gamma_{ij\ell}(\omega)$ has the required symmetry for gyration and that it forms an antisymmetric tensor of rank 3 (see Section 1.1.4.5.3 for the properties of antisymmetric tensors).

1.6.5.4. *Gyration tensor*

It is convenient to rewrite the effective dielectric expression in the following way (just keeping the first two terms):

$$\varepsilon_{ij}(\omega, \mathbf{k}) = \varepsilon_{ij}(\omega) + i\hat{e}_{ijm}g_{m\ell}k_l, \tag{1.6.5.12}$$

where $\hat{e}_{ijm}$ is a unit antisymmetric pseudotensor of rank 3 or permutation tensor ($\hat{e}_{123} = 1$, $\hat{e}_{213} = -1$, $\hat{e}_{112} = 0$ *etc.*; $\hat{e}_{ijm}$ is not affected by mirror reflection) and $g_{m\ell}$ represents a pseudotensor (*i.e.* axial tensor) of rank 2. One can then write further

$$\varepsilon_{ij}(\omega, \mathbf{k}) = \varepsilon_{ij}(\omega) + i\hat{e}_{ijm}G_m, \tag{1.6.5.13}$$

where $G_m = g_{m\ell}k_\ell$ is a component of a pseudovector (*i.e.* axial vector), known as the gyration vector. The formula for the dielectric displacement can then be expressed in the form

$$D_i = \varepsilon_o\varepsilon_{ij}(\omega, \mathbf{k})E_j = \varepsilon_o\big[\varepsilon_{ij}(\omega)E_j - i(\mathbf{G} \times \mathbf{E})_i\big]. \tag{1.6.5.14}$$

The operation $\mathbf{G} \times \mathbf{E}$ can also be represented by the product of an antisymmetric tensor $[G]$ with the vector $\mathbf{E}$:

$$\begin{pmatrix} 0 & G_{12} & G_{13} \\ -G_{12} & 0 & G_{23} \\ -G_{13} & -G_{23} & 0 \end{pmatrix}\begin{pmatrix} E_1 \\ E_2 \\ E_3 \end{pmatrix} = \begin{pmatrix} G_{12}E_2 + G_{13}E_3 \\ G_{23}E_3 - G_{12}E_1 \\ -G_{13}E_1 - G_{23}E_2 \end{pmatrix} = \begin{pmatrix} -G_3E_2 + G_2E_3 \\ -G_1E_3 + G_3E_1 \\ -G_2E_1 + G_1E_2 \end{pmatrix}, \tag{1.6.5.15}$$

where $-G_1 = G_{23} = -G_{32}$, $-G_2 = -G_{13} = G_{31}$ and $-G_3 = G_{12} = -G_{21}$. If $\hat{\mathbf{s}}$ is the unit vector in the propagation direction, then

$$\mathbf{G} = G\hat{\mathbf{s}} \tag{1.6.5.16}$$

and G represents the magnitude of the gyration vector. Thus,

$$\hat{\mathbf{s}} \cdot \mathbf{G} = \hat{\mathbf{s}} \cdot G\hat{\mathbf{s}} = G\hat{\mathbf{s}} \cdot \hat{\mathbf{s}} = G. \tag{1.6.5.17}$$

Consequently, if one knows the direction of propagation inside the crystal, the coefficient G can be calculated *via*

$$G = \hat{s}_1G_1 + \hat{s}_2G_2 + \hat{s}_3G_3 \tag{1.6.5.18}$$

and then the optical *rotatory power* is defined as

$$\rho = \frac{\pi G}{\lambda n}, \tag{1.6.5.19}$$

where ρ is the angle of rotation in degrees per millimetre. According to the way in which the sign of G has been defined here, a positive value of ρ means dextrorotation and a negative value means laevorotation.

There is a possibility of confusion here in terminology with respect to the term 'gyration tensor'. It is seen that there exists an antisymmetric tensor $[G]$: this is sometimes referred to as the gyration tensor. However, returning to equation (1.6.5.12), it is the pseudotensor given by $g_{m\ell}$ that is more often described as the gyration tensor. The difference between them is really one of emphasis. The $[G]$ tensor refers to the polarization directions of the wave, whereas the g tensor is referred to the direction of wave propagation. Thus, for example, G_{23} refers to a wave whose polarization lies in the x_2x_3 plane, and so propagates in the x_1 direction, according to the axial gyration vector component $-G_1$. The gyration is equally described by the tensor component g_{11}. Being an axial tensor, g_{11} corresponds to a wave travelling along x_1, along which direction one observes a rotation in the x_2x_3 plane.

Although g is in general an antisymmetric tensor, since it is only the scalar products $g_{m\ell}\hat{s}_m\hat{s}_\ell$ that are important in determining the rotation of the plane of polarization, the components of $\mathbf{D}$, and hence the refractive index behaviour, are independent of the antisymmetric part of $g_{m\ell}$. It is thus possible to construct a table of tensor invariances for the symmetric part of the gyration tensor with regard to the possible symmetry classes of a crystal (Table 1.6.5.1). For a discussion of the importance of the antisymmetric terms, see Agranovich & Ginzburg (1984).

1.6.5.5. *Optical rotation along the optic axis of a uniaxial crystal*

Consider a uniaxial crystal such as quartz, crystallizing in point group 32. In this case, the only dielectric tensor terms (for the effect of symmetry, see Section 1.1.4.10) are $\varepsilon_{11} = \varepsilon_{22} \neq \varepsilon_{33}$, with the off-diagonal terms equal to zero. The equations for the dielectric displacements along the three coordinate axes x_1, x_2 and x_3 are then given, according to equations (1.6.5.14) and (1.6.5.15), by

Table 1.6.5.1. *Symmetry constraints (see Section 1.1.4.10) on the gyration tensor g_{ij}*

All g_{ij} components are zero for the centrosymmetric point groups plus $4mm$, $\bar{4}3m$, $3m$, $6mm$, $\bar{6}$ and $\bar{6}m2$.

Triclinic	Monoclinic		Orthorhombic
Point group 1	Point group 2 ($2 \parallel x_2$)	Point group m ($m \perp x_2$)	Point group 222
$\begin{pmatrix} g_{11} & g_{12} & g_{13} \\ g_{12} & g_{22} & g_{23} \\ g_{13} & g_{23} & g_{33} \end{pmatrix}$	$\begin{pmatrix} g_{11} & 0 & g_{13} \\ 0 & g_{22} & 0 \\ g_{13} & 0 & g_{33} \end{pmatrix}$	$\begin{pmatrix} 0 & g_{12} & 0 \\ g_{12} & 0 & g_{23} \\ 0 & g_{23} & 0 \end{pmatrix}$	$\begin{pmatrix} g_{11} & 0 & 0 \\ 0 & g_{22} & 0 \\ 0 & 0 & g_{33} \end{pmatrix}$
	Point group 2 ($2 \parallel x_3$)	Point group m ($m \perp x_3$)	Point group $mm2$
	$\begin{pmatrix} g_{11} & g_{12} & 0 \\ g_{12} & g_{22} & 0 \\ 0 & 0 & g_{33} \end{pmatrix}$	$\begin{pmatrix} 0 & & g_{13} \\ & 0 & g_{23} \\ g_{13} & g_{23} & 0 \end{pmatrix}$	$\begin{pmatrix} 0 & g_{12} & 0 \\ g_{12} & 0 & 0 \\ 0 & 0 & 0 \end{pmatrix}$

Tetragonal		Trigonal and hexagonal	Cubic and isotropic
Point groups 4, 422	Point group $\bar{4}$	Point groups 3, 32, 6, 622	Point groups 432, 23
$\begin{pmatrix} g_{11} & 0 & 0 \\ 0 & g_{11} & 0 \\ 0 & 0 & g_{33} \end{pmatrix}$	$\begin{pmatrix} g_{11} & g_{12} & 0 \\ g_{12} & -g_{11} & 0 \\ 0 & 0 & 0 \end{pmatrix}$	$\begin{pmatrix} g_{11} & 0 & 0 \\ 0 & g_{11} & 0 \\ 0 & 0 & g_{33} \end{pmatrix}$	$\begin{pmatrix} g_{11} & 0 & 0 \\ 0 & g_{11} & 0 \\ 0 & 0 & g_{11} \end{pmatrix}$
Point group $\bar{4}2m$			Isotropic, no centre of symmetry
$\begin{pmatrix} g_{11} & 0 & 0 \\ 0 & -g_{11} & 0 \\ 0 & 0 & 0 \end{pmatrix}$			$\begin{pmatrix} g_{11} & 0 & 0 \\ 0 & g_{11} & 0 \\ 0 & 0 & g_{11} \end{pmatrix}$

$$\begin{aligned} D_1 &= \varepsilon_o \varepsilon_{11} E_1 - i\varepsilon_o \big[G_{12} E_2 + G_{13} E_3\big] \\ D_2 &= \varepsilon_o \varepsilon_{22} E_2 - i\varepsilon_o \big[G_{23} E_3 - G_{21} E_1\big] \\ D_3 &= \varepsilon_o \varepsilon_{33} E_3 - i\varepsilon_o \big[G_{31} E_1 - G_{32} E_2\big]. \end{aligned} \tag{1.6.5.20}$$

If the light is taken to propagate along x_3, the optic axis, the fundamental optics equation (1.6.3.14) is expressed as

$$\begin{aligned} &\begin{pmatrix} \varepsilon_{11} & -iG_{12} & -iG_{13} \\ iG_{12} & \varepsilon_{11} & -iG_{23} \\ iG_{13} & iG_{23} & \varepsilon_{33} + n^2 \end{pmatrix} \begin{pmatrix} E_1 \\ E_2 \\ E_3 \end{pmatrix} \\ &= \begin{pmatrix} n^2 & 0 & 0 \\ 0 & n^2 & 0 \\ 0 & 0 & n^2 \end{pmatrix} \begin{pmatrix} E_1 \\ E_2 \\ E_3 \end{pmatrix}. \end{aligned} \tag{1.6.5.21}$$

As usual, the longitudinal solution given by

$$iG_{13} E_1 + iG_{23} E_2 + \varepsilon_{33} E_3 = 0 \tag{1.6.5.22}$$

can be ignored, as one normally deals with a transverse electric field in the normal case of propagating light. For a non-trivial solution, then,

$$\begin{vmatrix} \varepsilon_{11} - n^2 & -iG_{12} \\ iG_{12} & \varepsilon_{11} - n^2 \end{vmatrix} = 0, \tag{1.6.5.23}$$

which gives

$$n^2 = \varepsilon_{11} \pm G_{12}. \tag{1.6.5.24}$$

This results in two eigenvalue solutions, n_1 and n_2, from which one has

$$(n_1 - n_2)(n_1 + n_2) = 2G_{12} = -2G_3 \tag{1.6.5.25}$$

and thus

$$n_1 - n_2 = \frac{G_{12}}{\bar{n}} = -\frac{G_3}{\bar{n}}. \tag{1.6.5.26}$$

The optical rotatory power (1.6.5.19) is then given by

$$\rho = \frac{\pi G_3}{\lambda \bar{n}} = \frac{\pi (n_2 - n_1)}{\lambda}. \tag{1.6.5.27}$$

Note that in order to be consistent with the definition of rotatory power used here, $n_2 > n_1$ for a dextrorotatory solution. This implies that n_2 should be identified with n_L and n_1 with n_R. To check this, find the eigenvectors corresponding to the two solutions (1.6.5.24).

For $n_1^2 = \varepsilon_{11} - G_3$, the following matrix is found from (1.6.5.21):

$$\begin{pmatrix} G_3 & iG_3 \\ -iG_3 & G_3 \end{pmatrix} = 0, \tag{1.6.5.28}$$

giving the Jones matrix

$$(1/2^{1/2}) \begin{pmatrix} 1 \\ -i \end{pmatrix} = 0. \tag{1.6.5.29}$$

This corresponds to a right-circularly polarized wave. It should be noted that there is confusion in the optics textbooks over the Jones matrices for circular polarizations. Jones (1948) writes a right-circular wave as

$$\begin{pmatrix} 1 \\ i \end{pmatrix},$$

but this is for a definition of right-circularly polarized light as that for which an instantaneous picture of the space distribution of its electric vector describes a right spiral. The modern usage is to define the sense of circular polarization through the time variation of the electric vector in a given plane as seen by an observer

looking towards the source of the light. This reverses the definition given by Jones.

For $n_2^2 = \varepsilon_{11} + G_3$, the following matrix is found:

$$\begin{pmatrix} -G_3 & iG_3 \\ -iG_3 & -G_3 \end{pmatrix} = 0, \tag{1.6.5.30}$$

giving

$$(1/2^{1/2})\begin{pmatrix} 1 \\ i \end{pmatrix} = 0. \tag{1.6.5.31}$$

This corresponds to a left-circularly polarized wave. Therefore it is proved that the optical rotation arises from a competition between two circularly polarized waves and that in equation (1.6.5.26) $n_1 = n_R$ and $n_2 = n_L$, the refractive indices for right- and left-circularly polarized light, respectively. Note that Fresnel's original idea of counter-rotating circular polarizations fits nicely with the eigenvectors rigorously determined in (1.6.5.29) and (1.6.5.31). Thus

$$\rho = \frac{\pi(n_L - n_R)}{\lambda}. \tag{1.6.5.32}$$

Finally, for light propagating along x_3 in quartz, one can write the direction of the wave normal as

$$\hat{s}_1 = 0; \quad \hat{s}_2 = 0; \quad \hat{s}_3 = 1 \tag{1.6.5.33}$$

and then the gyration vector is given by

$$G = g_{i3}\hat{s}_i\hat{s}_3 = g_{13} + g_{23} + g_{33} = g_{33} \tag{1.6.5.34}$$

as $g_{12} = g_{23} = 0$ in point group 32. Thus from (1.6.5.26) it is seen that

$$g_{33} = G_3 = -G_{12}, \tag{1.6.5.35}$$

thus linking one of the components of the gyration tensor $g_{m\ell}$ with a component of the gyration vector **G** and a tensor component of $[G]$.

1.6.5.6. *Optical rotation perpendicular to the optic axis of a uniaxial crystal*

The magnitude of circular birefringence is typically about 10^{-4} times smaller than that of linear birefringence. For this reason, optical rotation has usually been observed only in directions where the linear birefringence is absent, such as in optic axial directions. However, it has been clear for some time that optical rotation also exists in other directions and that with specialized techniques it is even possible to measure it. The techniques (Moxon & Renshaw, 1990; Moxon *et al.*, 1991) are complex and require very precise measuring capabilities, and therefore are generally not commonly available.

Probably the best known case where optical rotation has been measured in a linearly birefringent section is that of quartz. It has been seen that it is easy to measure the rotation along the optic axial direction, since this is the direction along which the crystal looks isotropic. Szivessy & Münster (1934) measured the rotation in a direction perpendicular to the optic axis and found that its magnitude was smaller and opposite in sign to that along the optic axis of the same crystal.

To see the relationship between the linear and circular birefringences, consider light travelling along x_1 in quartz. The fundamental equation (1.6.3.14) then becomes

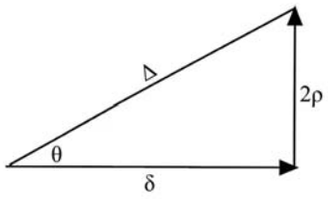

Fig. 1.6.5.3. The principle of superposition.

$$\begin{pmatrix} \varepsilon_{11} - n^2 & -iG_{12} & -iG_{13} \\ iG_{12} & \varepsilon_{11} & -iG_{23} \\ iG_{13} & iG_{23} & \varepsilon_{33} \end{pmatrix}\begin{pmatrix} E_1 \\ E_2 \\ E_3 \end{pmatrix} = \begin{pmatrix} n^2 & 0 & 0 \\ 0 & n^2 & 0 \\ 0 & 0 & n^2 \end{pmatrix}\begin{pmatrix} E_1 \\ E_2 \\ E_3 \end{pmatrix}. \tag{1.6.5.36}$$

Solving for the non-trivial transverse solutions

$$\begin{vmatrix} \varepsilon_{11} - n^2 & -iG_{23} \\ iG_{23} & \varepsilon_{33} - n^2 \end{vmatrix} = 0 \tag{1.6.5.37}$$

and then

$$n^4 - n^2(\varepsilon_{11} + \varepsilon_{33}) + \varepsilon_{11}\varepsilon_{33} - G_{23}^2 = 0. \tag{1.6.5.38}$$

Finding the roots of this equation considered as a quadratic in n^2, the following birefringence is obtained:

$$n_1 - n_2 = \left[(n_o - n_e)^2 + (G_{23}^2/\bar{n}^2)\right]^{1/2}. \tag{1.6.5.39}$$

The eigenvectors for the two solutions n_1 and n_2 can easily be shown to correspond to elliptical polarizations. Notice that in equation (1.6.5.39), two refractive-index solutions are obtained whose difference depends on two terms, one with respect to the linear birefringence $n_o - n_e$ and the other to the circular birefringence represented by the gyration component $G_{23} = -G_1$. The refractive-index difference $n_1 - n_2$ gives rise to a phase shift between the two elliptically polarized components of the light, given by

$$\Delta = (2\pi/\lambda)(n_1 - n_2), \tag{1.6.5.40}$$

from which

$$\Delta^2 = (4\pi^2/\lambda^2)\left[(n_o - n_e)^2 + (G_{23}^2/\bar{n}^2)\right] = \delta^2 + (2\rho)^2, \tag{1.6.5.41}$$

where

$$\delta = \frac{2\pi}{\lambda}(n_o - n_e) \quad \text{and} \quad \rho = \frac{-\pi G_{23}}{\lambda\bar{n}} = \frac{-\pi G_1}{\lambda\bar{n}}. \tag{1.6.5.42}$$

δ is the phase difference when there is no optical rotation and 2ρ is the phase difference corresponding to a normal optical rotation ρ when there is no linear birefringence. (1.6.5.41) shows that the linear and circular terms simply add, and this is known as the *principle of superposition*.

This reveals that an elliptical polarization is created by the simple vector addition of a linearly polarized wave to a circularly polarized wave, as indicated in Fig. 1.6.5.3. From this, the ellipticity κ of the polarization is given by

$$\kappa = \tan(\tfrac{1}{2}\theta), \tag{1.6.5.43}$$

where

$$\tan\theta = \frac{2\rho}{\delta}. \tag{1.6.5.44}$$

Table 1.6.6.1. *Symmetry constraints (see Section 1.1.4.10) on the linear electro-optic tensor r_{ij} (contracted notation)*

Triclinic	Monoclinic		Orthorhombic
Point group 1	Point group 2 ($2 \parallel x_2$)	Point group m ($m \perp x_2$)	Point group 222
$\begin{pmatrix} r_{11} & r_{12} & r_{13} \\ r_{21} & r_{22} & r_{23} \\ r_{31} & r_{32} & r_{33} \\ r_{41} & r_{42} & r_{43} \\ r_{51} & r_{52} & r_{53} \\ r_{61} & r_{62} & r_{63} \end{pmatrix}$	$\begin{pmatrix} 0 & r_{12} & 0 \\ 0 & r_{22} & 0 \\ 0 & r_{32} & 0 \\ r_{41} & 0 & r_{43} \\ 0 & r_{52} & 0 \\ r_{61} & 0 & r_{63} \end{pmatrix}$	$\begin{pmatrix} r_{11} & 0 & r_{13} \\ r_{21} & 0 & r_{23} \\ r_{31} & 0 & r_{33} \\ 0 & r_{42} & 0 \\ r_{51} & 0 & r_{53} \\ 0 & r_{62} & 0 \end{pmatrix}$	$\begin{pmatrix} 0 & 0 & 0 \\ 0 & 0 & 0 \\ 0 & 0 & 0 \\ r_{41} & 0 & 0 \\ 0 & r_{52} & 0 \\ 0 & 0 & r_{63} \end{pmatrix}$
	Point group 2 ($2 \parallel x_3$)	Point group m ($m \perp x_3$)	Point group $mm2$
	$\begin{pmatrix} 0 & 0 & r_{13} \\ 0 & 0 & r_{23} \\ 0 & 0 & r_{33} \\ r_{41} & r_{42} & 0 \\ r_{51} & r_{52} & 0 \\ 0 & 0 & r_{63} \end{pmatrix}$	$\begin{pmatrix} r_{11} & r_{12} & 0 \\ r_{21} & r_{22} & 0 \\ r_{31} & r_{32} & 0 \\ 0 & 0 & r_{43} \\ 0 & 0 & r_{53} \\ r_{61} & r_{62} & 0 \end{pmatrix}$	$\begin{pmatrix} 0 & 0 & r_{13} \\ 0 & 0 & r_{23} \\ 0 & 0 & r_{33} \\ 0 & r_{42} & 0 \\ r_{51} & 0 & 0 \\ 0 & 0 & 0 \end{pmatrix}$

Tetragonal		Trigonal	
Point group 4	Point group $\bar{4}$	Point group 3	Point group 32
$\begin{pmatrix} 0 & 0 & r_{13} \\ 0 & 0 & r_{13} \\ 0 & 0 & r_{33} \\ r_{41} & r_{51} & 0 \\ r_{51} & -r_{41} & 0 \\ 0 & 0 & 0 \end{pmatrix}$	$\begin{pmatrix} 0 & 0 & r_{13} \\ 0 & 0 & -r_{13} \\ 0 & 0 & 0 \\ r_{41} & -r_{51} & 0 \\ r_{51} & r_{41} & 0 \\ 0 & 0 & r_{63} \end{pmatrix}$	$\begin{pmatrix} r_{11} & -r_{22} & r_{13} \\ -r_{11} & r_{22} & r_{13} \\ 0 & 0 & r_{33} \\ r_{41} & r_{51} & 0 \\ r_{51} & -r_{41} & 0 \\ -r_{22} & -r_{11} & 0 \end{pmatrix}$	$\begin{pmatrix} r_{11} & 0 & 0 \\ -r_{11} & 0 & 0 \\ 0 & 0 & 0 \\ r_{41} & 0 & 0 \\ 0 & -r_{41} & 0 \\ 0 & -r_{11} & 0 \end{pmatrix}$
Point group $\bar{4}2m$	Point group 422	Point group $3m1$ ($m \perp x_1$)	Point group $31m$ ($m \perp x_2$)
$\begin{pmatrix} 0 & 0 & 0 \\ 0 & 0 & 0 \\ 0 & 0 & 0 \\ r_{41} & & 0 \\ & r_{41} & 0 \\ 0 & 0 & r_{63} \end{pmatrix}$	$\begin{pmatrix} 0 & 0 & 0 \\ 0 & 0 & 0 \\ 0 & 0 & 0 \\ r_{41} & 0 & 0 \\ 0 & -r_{41} & 0 \\ 0 & 0 & 0 \end{pmatrix}$	$\begin{pmatrix} 0 & -r_{22} & r_{13} \\ 0 & r_{22} & r_{13} \\ 0 & 0 & r_{33} \\ 0 & r_{51} & 0 \\ r_{51} & 0 & 0 \\ -r_{22} & 0 & 0 \end{pmatrix}$	$\begin{pmatrix} r_{11} & 0 & r_{13} \\ -r_{11} & 0 & r_{13} \\ 0 & 0 & r_{33} \\ 0 & r_{51} & 0 \\ r_{51} & 0 & 0 \\ 0 & -r_{11} & 0 \end{pmatrix}$
Point group $4mm$			
$\begin{pmatrix} 0 & 0 & r_{13} \\ 0 & 0 & r_{13} \\ 0 & 0 & r_{33} \\ 0 & r_{51} & 0 \\ r_{51} & 0 & 0 \\ 0 & 0 & 0 \end{pmatrix}$			

Hexagonal			Cubic
Point group 6	Point group $6mm$	Point group 622	Point groups $\bar{4}3m$, 23
$\begin{pmatrix} 0 & 0 & r_{13} \\ 0 & 0 & r_{13} \\ 0 & 0 & r_{33} \\ r_{41} & r_{51} & 0 \\ r_{51} & -r_{41} & 0 \\ 0 & 0 & 0 \end{pmatrix}$	$\begin{pmatrix} 0 & 0 & r_{13} \\ 0 & 0 & r_{13} \\ 0 & 0 & r_{33} \\ 0 & r_{51} & 0 \\ r_{51} & 0 & 0 \\ 0 & 0 & 0 \end{pmatrix}$	$\begin{pmatrix} 0 & 0 & 0 \\ 0 & 0 & 0 \\ 0 & 0 & 0 \\ r_{41} & 0 & 0 \\ 0 & -r_{41} & 0 \\ 0 & 0 & 0 \end{pmatrix}$	$\begin{pmatrix} 0 & 0 & 0 \\ 0 & 0 & 0 \\ 0 & 0 & 0 \\ r_{41} & 0 & 0 \\ 0 & r_{41} & 0 \\ 0 & 0 & r_{41} \end{pmatrix}$
Point group $\bar{6}$	Point group $\bar{6}m2$ ($m \perp x_1$)	Point group $\bar{6}2m$ ($m \perp x_2$)	Point group 432
$\begin{pmatrix} r_{11} & -r_{22} & 0 \\ -r_{11} & r_{22} & 0 \\ 0 & 0 & 0 \\ 0 & 0 & 0 \\ 0 & 0 & 0 \\ -r_{22} & -r_{11} & 0 \end{pmatrix}$	$\begin{pmatrix} 0 & -r_{22} & 0 \\ 0 & r_{22} & 0 \\ 0 & 0 & 0 \\ 0 & 0 & 0 \\ 0 & 0 & 0 \\ -r_{22} & 0 & 0 \end{pmatrix}$	$\begin{pmatrix} r_{11} & 0 & 0 \\ -r_{11} & 0 & 0 \\ 0 & 0 & 0 \\ 0 & 0 & 0 \\ 0 & 0 & 0 \\ 0 & -r_{11} & 0 \end{pmatrix}$	$\begin{pmatrix} 0 & 0 & 0 \\ 0 & 0 & 0 \\ 0 & 0 & 0 \\ 0 & 0 & 0 \\ 0 & 0 & 0 \\ 0 & 0 & 0 \end{pmatrix}$

Thus

$$\tan\theta = \frac{G_1}{\bar{n}(n_o - n_e)} = \frac{g_{11}}{\bar{n}(n_o - n_e)}. \qquad (1.6.5.45)$$

Generally speaking, the ellipticity is extremely small and difficult to measure (Moxon & Renshaw, 1990). In right-handed quartz (right-handed with respect to optical rotation observed along the c axis), $n_o = 1.544$, $n_e = 1.553$, $g_{11} = g_{22} = -5.82 \times 10^{-5}$ and $g_{33} = 12.96 \times 10^{-5}$ measured at $\lambda = 5100$ Å. Since the c axis is also the optic axis, $\delta = 0$ for the (0001) plane, and thus $\kappa = 1$ for this section [equations (1.6.5.44) and (1.6.5.43)]. This value of $\kappa = 1$ means that the two waves are circular (see Section 1.6.5.5), *i.e.* there is no linear birefringence, only a pure rotation. In this direction, the gyration g_{33} means a rotation of $\rho = 29.5^\circ\ \text{mm}^{-1}$ [using equation (1.6.5.27)]. In a direction normal to the optic axis, from equation (1.6.5.40) one finds $\rho = -13.3^\circ\ \text{mm}^{-1}$. However, in this direction, the crystal appears linearly birefringent with $\delta = 110.88\ \text{mm}^{-1}$ [equation (1.6.5.42)]. Thus the ellipticity $\kappa = -0.00209$, as calculated from equations (1.6.5.44) and (1.6.5.43). In other words, the two waves are very slightly elliptical, and the sense of rotation of the two ellipses is reversed. Because of the change in sign of the gyration coefficients, it is found that at an angle of $56^\circ\ 10'$ down from the optic axis $\kappa = 0$, meaning that waves travelling along this direction show no optical rotation, only linear birefringence.

1.6.6. Linear electro-optic effect

The linear electro-optic effect, given by $P_i^\omega = \varepsilon_o \chi_{ijk} E_j^\omega E_k^0$, is conventionally expressed in terms of the change in dielectric impermeability caused by imposition of a static electric field on the crystal. Thus one may write the linear electro-optic effect as

$$\Delta\eta_{ij} = r_{ijk} E_k^0, \qquad (1.6.6.1)$$

where the coefficients r_{ijk} form the so-called *linear electro-optic tensor*. These have identical symmetry with the piezoelectric tensor and so obey the same rules (see Table 1.6.6.1). Like the piezoelectric tensor, there is a maximum of 18 independent coefficients (triclinic case) (see Section 1.1.4.10.3). However, unlike in piezoelectricity, in using the Voigt contracted notation there are two major differences:

(1) In writing the electro-optic tensor components as r_{ij}, the first suffix refers to the column number and the second suffix is the row number.

(2) There are no factors of 1/2 or 2.

Typical values of linear electro-optic coefficients are around $10^{-12}\ \text{mV}^{-1}$.

1.6.6.1. *Primary and secondary effects*

In considering the electro-optic effect, it is necessary to bear in mind that, in addition to the primary effect of changing the refractive index, the applied electric field may also cause a strain in the crystal *via* the converse piezoelectric effect, and this can then change the refractive index, as a secondary effect, through the elasto-optic effect. Both these effects, which are of comparable magnitude in practice, will occur if the crystal is free. However, if the crystal is mechanically clamped, it is not possible to induce any strain, and in this case therefore only the primary electro-optic effect is seen. In practice, the free and clamped behaviour can be investigated by measuring the linear birefringence when applying electric fields of varying frequencies. When the electric field is static or of low frequency, the effect is measured at constant stress, so that both primary and secondary effects are measured together. For electric fields at frequencies above the natural mechanical resonance of the crystal, the strains are very small, and in this case only the primary effect is measured.

1.6.6.2. *Example of $LiNbO_3$*

In order to understand how tensors can be used in calculating the optical changes induced by an applied electric field, it is instructive to take a particular example and work out the change in refractive index for a given electric field. $LiNbO_3$ is the most widely used electro-optic material in industry and so this forms a useful example for calculation purposes. This material crystallizes in point group $3m$, for which the electro-optic tensor has the form (for the effect of symmetry, see Section 1.1.4.10) (with x_1 perpendicular to m)

$$\begin{pmatrix} 0 & -r_{22} & r_{13} \\ 0 & r_{22} & r_{13} \\ 0 & 0 & r_{33} \\ 0 & r_{51} & 0 \\ r_{51} & 0 & 0 \\ -r_{22} & 0 & 0 \end{pmatrix}, \qquad (1.6.6.2)$$

with $r_{13} = 9.6$, $r_{22} = 6.8$, $r_{33} = 30.9$ and $r_{51} = 32.5 \times 10^{-12}\ \text{mV}^{-1}$, under the normal measuring conditions where the crystal is unclamped.

Calculation using dielectric impermeability tensor. Suppose, for example, a static electric field E_3^0 is imposed along the x_3 axis. One can then write

$$\begin{pmatrix} \Delta\eta_1 \\ \Delta\eta_2 \\ \Delta\eta_3 \\ \Delta\eta_4 \\ \Delta\eta_5 \\ \Delta\eta_6 \end{pmatrix} = \begin{pmatrix} 0 & -r_{22} & r_{13} \\ 0 & r_{22} & r_{13} \\ 0 & 0 & r_{33} \\ 0 & r_{51} & 0 \\ r_{51} & 0 & 0 \\ -r_{22} & 0 & 0 \end{pmatrix} \begin{pmatrix} 0 \\ 0 \\ E_3^0 \end{pmatrix} = \begin{pmatrix} r_{13}E_3^0 \\ r_{13}E_3^0 \\ r_{33}E_3^0 \\ 0 \\ 0 \\ 0 \end{pmatrix}. \qquad (1.6.6.3)$$

Thus

$$\begin{aligned} \Delta\eta_1 &= r_{13}E^0 = \Delta\eta_2 \\ \Delta\eta_3 &= r_{33}E^0 \\ \Delta\eta_4 &= \Delta\eta_5 = \Delta\eta_6 = 0. \end{aligned} \qquad (1.6.6.4)$$

Since the original indicatrix of $LiNbO_3$ before application of the field is uniaxial,

$$\begin{aligned} \eta_1 &= \frac{1}{n_o^2} = \eta_2 \\ \eta_3 &= \frac{1}{n_e^2}, \end{aligned} \qquad (1.6.6.5)$$

and so differentiating, the following are obtained:

$$\begin{aligned} \Delta\eta_1 &= \Delta\eta_2 = -\frac{2}{n_o^3}\Delta n_o \\ \Delta\eta_3 &= -\frac{2}{n_e^3}\Delta n_e. \end{aligned} \qquad (1.6.6.6)$$

Thus, the induced changes in refractive index are given by

$$\begin{aligned} \Delta n_1 &= \Delta n_2 = -\frac{n_o^3}{2} r_{13} E_3^0 \\ \Delta n_3 &= -\frac{n_e^3}{2} r_{33} E_3^0. \end{aligned} \qquad (1.6.6.7)$$

It can be seen from this that the effect is simply to change the refractive indices by deforming the indicatrix, but maintain the uniaxial symmetry of the crystal. Note that if light is now propagated along, say, x_1, the observed linear birefringence is given by

$$(n_e - n_o) - \tfrac{1}{2}(n_e^3 r_{33} - n_o^3 r_{13}) E_3^0. \qquad (1.6.6.8)$$

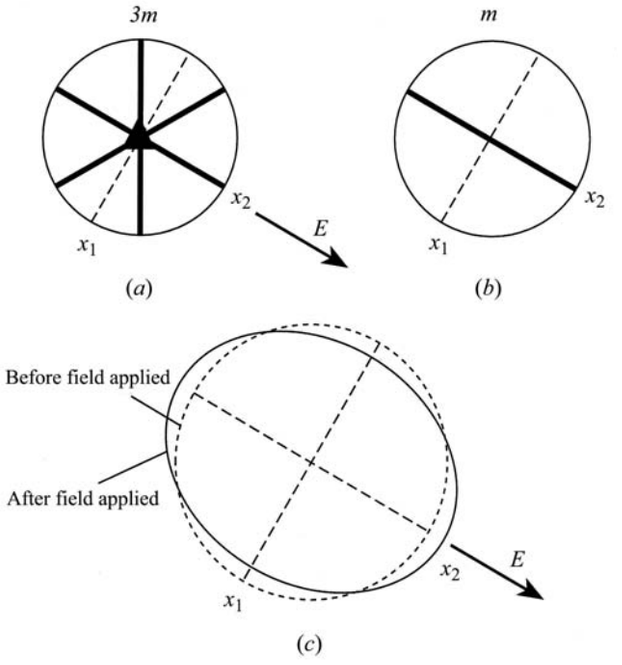

Fig. 1.6.6.1. (*a*) Symmetry elements of point group 3*m*. (*b*) Symmetry elements after field applied along x_2. (*c*) Effect on circular section of uniaxial indicatrix.

If, on the other hand, the electric field E_2^0 is applied along x_2, *i.e.* within the mirror plane, one finds

$$\begin{aligned}\Delta\eta_1 &= -r_{22}E_2^0\\ \Delta\eta_2 &= +r_{22}E_2^0\\ \Delta\eta_4 &= +r_{51}E_2^0\\ \Delta\eta_3 &= \Delta\eta_5 = \Delta\eta_6 = 0.\end{aligned} \tag{1.6.6.9}$$

Diagonalization of the matrix

$$\begin{pmatrix}\Delta\eta_1 & 0 & 0\\ 0 & \Delta\eta_2 & \Delta\eta_4\\ 0 & \Delta\eta_4 & \Delta\eta_3\end{pmatrix} \tag{1.6.6.10}$$

containing these terms gives three eigenvalue solutions for the changes in dielectric impermeabilities:

$$\begin{aligned}&(1) && -r_{22}E_2^0\\ &(2) && \frac{r_{22}+(r_{22}^2+4r_{51}^2)^{1/2}}{2}E_2^0\\ &(3) && \frac{r_{22}-(r_{22}^2+4r_{51}^2)^{1/2}}{2}E_2^0.\end{aligned} \tag{1.6.6.11}$$

On calculating the eigenfunctions, it is found that solution (1) lies along x_1, thus representing a change in the value of the indicatrix axis in this direction. Solutions (2) and (3) give the other two axes of the indicatrix: these are different in length, but mutually perpendicular, and lie in the x_2x_3 plane. Thus a biaxial indicatrix is formed with one refractive index fixed along x_1 and the other two in the plane perpendicular. The effect of having the electric field imposed within the mirror plane is thus to remove the threefold axis in point group 3*m* and to form the point subgroup *m* (Fig. 1.6.6.1).

Relationship between linear electro-optic coefficients r_{ijk} and the susceptibility tensor $\chi^{(2)}_{ijk}$. It is instructive to repeat the above calculation using the normal susceptibility tensor and equation (1.6.3.14). Consider, again, a static electric field along x_3 and light propagating along x_1. As before, the only coefficients that need to be considered with the static field along x_3 are $\chi_{113} = \chi_{223}$ and χ_{333}. Equation (1.6.3.14) can then be written as

$$\begin{pmatrix}\varepsilon_1+\varepsilon_o\chi_{13}E_3^0+n^2 & 0 & 0\\ 0 & \varepsilon_1+\varepsilon_o\chi_{13}E_3^0 & 0\\ 0 & 0 & \varepsilon_3+\varepsilon_o\chi_{33}E_3^0\end{pmatrix}\begin{pmatrix}E_1\\E_2\\E_3\end{pmatrix} = \begin{pmatrix}n^2 & 0 & 0\\ 0 & n^2 & 0\\ 0 & 0 & n^2\end{pmatrix}\begin{pmatrix}E_1\\E_2\\E_3\end{pmatrix}, \tag{1.6.6.12}$$

where for simplicity the Voigt notation has been used. The first line of the matrix equation gives

$$(\varepsilon_1+\varepsilon_o\chi_{13}E_3^0+n^2)E_1 = n^2E_1. \tag{1.6.6.13}$$

Since only a transverse electric field is relevant for an optical wave (plasma waves are not considered here), it can be assumed that the longitudinal field $E_1 = 0$. The remaining two equations can be solved by forming the determinantal equation

$$\begin{vmatrix}\varepsilon_1+\varepsilon_o\chi_{13}E_3^0-n^2 & 0\\ 0 & \varepsilon_3+\varepsilon_o\chi_{33}E_3^0-n^2\end{vmatrix} = 0, \tag{1.6.6.14}$$

which leads to the results

$$n_1^2 = \varepsilon_1+\varepsilon_o\chi_{13}E_3^0 \quad\text{and}\quad n_2^2 = \varepsilon_3+\varepsilon_o\chi_{33}E_3^0. \tag{1.6.6.15}$$

Thus

$$n_1^2 = n_o^2+\varepsilon_o\chi_{13}E_3^0 \quad\text{and}\quad n_2^2 = n_e^2+\varepsilon_o\chi_{33}E_3^0, \tag{1.6.6.16}$$

and so

$$(n_1-n_o)(n_1+n_o) = \varepsilon_o\chi_{13}E_3^0 \quad\text{and}\quad (n_2-n_e)(n_2+n_e) = \varepsilon_o\chi_{33}E_3^0, \tag{1.6.6.17}$$

and since $n_1 \simeq n_o$ and $n_2 \simeq n_e$,

$$n_1-n_o = \frac{\varepsilon_o\chi_{13}E_3^0}{2n_o} \quad\text{and}\quad n_2-n_e = \frac{\varepsilon_o\chi_{33}E_3^0}{2n_e}. \tag{1.6.6.18}$$

Subtracting these two results, the induced birefringence is found:

$$(n_e-n_o) - \tfrac{1}{2}\left(\frac{\varepsilon_o\chi_{33}}{n_e}-\frac{\varepsilon_o\chi_{13}}{n_o}\right)E_3^0. \tag{1.6.6.19}$$

Comparing with the equation (1.6.6.8) calculated for the linear electro-optic coefficients,

$$(n_e-n_o) - \tfrac{1}{2}\left(n_e^3r_{33}-n_o^3r_{13}\right)E_3^0, \tag{1.6.6.20}$$

one finds the following relationships between the linear electro-optic coefficients and the susceptibilities $\chi^{(2)}$:

$$r_{13} = \frac{\varepsilon_o\chi_{13}}{n_o^4} \quad\text{and}\quad r_{33} = \frac{\varepsilon_o\chi_{33}}{n_e^4}. \tag{1.6.6.21}$$

1.6.7. The linear photoelastic effect

1.6.7.1. *Introduction*

The linear photoelastic (or piezo-optic) effect (Narasimhamurty, 1981) is given by $P_i^\omega = \varepsilon_o\chi_{ijk\ell}E_j^\omega S_{k\ell}^0$, and, like the electro-optic effect, it can be discussed in terms of the change in dielectric impermeability caused by a static (or low-frequency) field, in this case a stress, applied to the crystal. This can be written in the form

$$\Delta\eta_{ij} = \pi_{ijk\ell}T_{k\ell}^0. \tag{1.6.7.1}$$

The coefficients $\pi_{ijk\ell}$ form a fourth-rank tensor known as the *linear piezo-optic* tensor. Typically, the piezo-optic coefficients are of the order of 10^{-12} m^2 N^{-1}. It is, however, more usual to express the effect as an *elasto-optic effect* by making use of the relationship between stress and strain (see Section 1.3.3.2), thus

$$T_{k\ell} = c_{k\ell mn} S_{mn}, \tag{1.6.7.2}$$

where the $c_{k\ell mn}$ are the elastic stiffness coefficients. Therefore equation (1.6.7.2) can be rewritten in the form

$$\Delta\eta_{ij} = \pi_{ijk\ell} c_{k\ell mn} S_{mn} = p_{ijmn} S_{mn} \tag{1.6.7.3}$$

or, in contracted notation,

$$\Delta\eta_i = p_{ij} S_j, \tag{1.6.7.4}$$

where, for convenience, the superscript 0 has been dropped, the elastic strain being considered as essentially static or of low frequency compared with the natural mechanical resonances of the crystal. The p_{ijmn} are coefficients that form the *linear elasto-optic* (or *strain-optic*) *tensor* (Table 1.6.7.1). Note that these coefficients are dimensionless, and typically of order 10^{-1}, showing that the change to the optical indicatrix is roughly one-tenth of the strain.

The elasto-optic effect can arise in several ways. The most obvious way is through application of an external stress, applied to the surfaces of the crystal. However, strains, and hence changes to the refractive indices, can arise in a crystal through other ways that are less obvious. Thus, it is a common finding that crystals can be twinned, and thus the boundary between twin domains, which corresponds to a mismatch between the crystal structures either side of the domain boundary, will exhibit a strain. Such a crystal, when viewed between crossed polars under a microscope will produce birefringence colours that will highlight the contrast between the domains. This is known as *strain birefringence*. Similarly, when a crystal undergoes a phase transition involving a change in crystal system, a so-called *ferroelastic transition*, there will be a change in strain owing to the difference in unit-cell shapes. Hence there will be a corresponding change in the optical indicatrix. Often the phase transition is one going from a high-temperature optically isotropic section to a low-temperature optically anisotropic section. In this case, the high-temperature section has no internal strain, but the low-temperature phase acquires a strain, which is often called the *spontaneous strain* (by analogy with the term spontaneous polarization in ferroelectrics).

1.6.7.2. *Spontaneous strain in $BaTiO_3$*

As an example of the calculation of the relationship between spontaneous strain and linear birefringence, consider the high-temperature phase transition of the well known perovskite $BaTiO_3$. This substance undergoes a transition at around 403 K on cooling from its high-temperature $Pm\bar{3}m$ phase to the room-temperature $P4mm$ phase. The $P4mm$ phase is both ferroelectric and ferroelastic. In this tetragonal phase, there is a small distortion of the unit cell along [001] and a contraction along $\langle 100\rangle$ compared with the unit cell of the high-temperature cubic phase, and so the room-temperature phase can be expected to have a uniaxial optical indicatrix.

The elasto-optic tensor for the $m\bar{3}m$ phase is (Table 1.6.7.1)

$$\begin{pmatrix} p_{11} & p_{12} & p_{12} & 0 & 0 & 0 \\ p_{12} & p_{11} & p_{12} & 0 & 0 & 0 \\ p_{12} & p_{12} & p_{11} & 0 & 0 & 0 \\ 0 & 0 & 0 & p_{44} & 0 & 0 \\ 0 & 0 & 0 & 0 & p_{44} & 0 \\ 0 & 0 & 0 & 0 & 0 & p_{44} \end{pmatrix}. \tag{1.6.7.5}$$

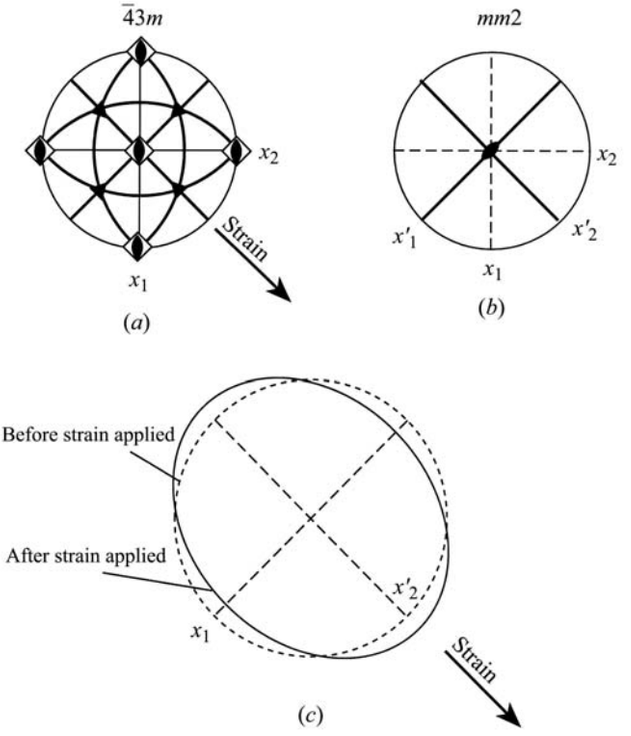

Fig. 1.6.7.1. (*a*) Symmetry elements of point group $\bar{4}3m$. (*b*) Symmetry elements after strain applied along [110]. (*c*) Effect on spherical indicatrix.

Consider the low-temperature tetragonal phase to arise as a small distortion of this cubic phase, with a spontaneous strain S_3^s given by the lattice parameters of the tetragonal phase:

$$S_3^s = [(c - a)/a]. \tag{1.6.7.6}$$

Therefore, the equations (1.6.7.4) for the dielectric impermeability in terms of the spontaneous strain component are given in matrix form as

$$\begin{aligned} \begin{pmatrix} \Delta\eta_1 \\ \Delta\eta_2 \\ \Delta\eta_3 \\ \Delta\eta_4 \\ \Delta\eta_5 \\ \Delta\eta_6 \end{pmatrix} &= \begin{pmatrix} p_{11} & p_{12} & p_{12} & 0 & 0 & 0 \\ p_{12} & p_{11} & p_{12} & 0 & 0 & 0 \\ p_{12} & p_{12} & p_{11} & 0 & 0 & 0 \\ 0 & 0 & 0 & p_{44} & 0 & 0 \\ 0 & 0 & 0 & 0 & p_{44} & 0 \\ 0 & 0 & 0 & 0 & 0 & p_{44} \end{pmatrix} \begin{pmatrix} 0 \\ 0 \\ S_3^s \\ 0 \\ 0 \\ 0 \end{pmatrix} \\ &= \begin{pmatrix} p_{12} S_3^s \\ p_{12} S_3^s \\ p_{11} S_3^s \\ 0 \\ 0 \\ 0 \end{pmatrix} \end{aligned} \tag{1.6.7.7}$$

so that

$$\begin{aligned} \Delta\eta_1 &= \Delta\eta_2 = p_{12} S_3^s \\ \Delta\eta_3 &= p_{11} S_3^s \\ \Delta\eta_4 &= \Delta\eta_5 = \Delta\eta_6 = 0. \end{aligned} \tag{1.6.7.8}$$

By analogy with equations (1.6.6.5) and (1.6.6.6), the induced changes in refractive index are then

Table 1.6.7.1. *Symmetry constraints on the linear elasto-optic (strain-optic) tensor p_{ij} (contracted notation) (see Section 1.1.4.10.6)*

Triclinic

Point group 1

$$\begin{pmatrix} p_{11} & p_{12} & p_{13} & p_{14} & p_{15} & p_{16} \\ p_{21} & p_{22} & p_{23} & p_{24} & p_{25} & p_{26} \\ p_{31} & p_{32} & p_{33} & p_{34} & p_{35} & p_{36} \\ p_{41} & p_{42} & p_{43} & p_{44} & p_{45} & p_{46} \\ p_{51} & p_{52} & p_{53} & p_{54} & p_{55} & p_{56} \\ p_{61} & p_{62} & p_{63} & p_{64} & p_{65} & p_{66} \end{pmatrix}$$

Orthorhombic

Point groups 222, *mm*2, *mmm*

$$\begin{pmatrix} p_{11} & p_{12} & p_{13} & 0 & 0 & 0 \\ p_{21} & p_{22} & p_{23} & 0 & 0 & 0 \\ p_{31} & p_{32} & p_{33} & 0 & 0 & 0 \\ 0 & 0 & 0 & p_{44} & 0 & 0 \\ 0 & 0 & 0 & & p_{55} & 0 \\ 0 & 0 & 0 & 0 & 0 & p_{66} \end{pmatrix}$$

Tetragonal

Point groups 4, $\bar{4}$, 4/*m*

$$\begin{pmatrix} p_{11} & p_{12} & p_{13} & 0 & 0 & p_{16} \\ p_{12} & p_{22} & p_{13} & 0 & 0 & -p_{16} \\ p_{31} & p_{31} & p_{33} & 0 & 0 & 0 \\ 0 & 0 & 0 & p_{44} & p_{45} & 0 \\ 0 & 0 & 0 & -p_{45} & p_{55} & 0 \\ p_{61} & -p_{61} & 0 & & 0 & p_{66} \end{pmatrix}$$

Point groups 4*mm*, $\bar{4}$2*m*, 422, 4/*mmm*

$$\begin{pmatrix} p_{11} & p_{12} & p_{13} & 0 & 0 & 0 \\ p_{12} & p_{22} & p_{13} & 0 & 0 & 0 \\ p_{31} & p_{31} & p_{33} & 0 & 0 & 0 \\ 0 & 0 & 0 & p_{44} & 0 & 0 \\ 0 & 0 & 0 & 0 & p_{44} & 0 \\ 0 & 0 & 0 & 0 & 0 & p_{66} \end{pmatrix}$$

Trigonal

Point groups 3, $\bar{3}$

$$\begin{pmatrix} p_{11} & p_{12} & p_{13} & p_{14} & p_{15} & p_{16} \\ p_{12} & p_{11} & p_{13} & -p_{14} & -p_{15} & -p_{16} \\ p_{31} & p_{31} & p_{33} & 0 & 0 & 0 \\ p_{41} & -p_{41} & 0 & p_{44} & p_{45} & -p_{51} \\ p_{51} & -p_{51} & 0 & -p_{44} & p_{44} & p_{41} \\ -p_{16} & p_{16} & 0 & -p_{15} & p_{14} & \tfrac{1}{2}(p_{11}-p_{12}) \end{pmatrix}$$

Point groups 3*m*, $\bar{3}$*m*, 32

$$\begin{pmatrix} p_{11} & p_{12} & p_{13} & p_{14} & 0 & 0 \\ p_{12} & p_{11} & p_{13} & -p_{14} & 0 & 0 \\ p_{13} & p_{13} & p_{33} & 0 & 0 & 0 \\ p_{41} & -p_{41} & 0 & p_{44} & 0 & 0 \\ 0 & 0 & 0 & 0 & p_{44} & p_{41} \\ 0 & 0 & 0 & 0 & p_{14} & \tfrac{1}{2}(p_{11}-p_{12}) \end{pmatrix}$$

Monoclinic

Point groups 2, *m*, 2/*m* (2 ∥ x_2)

$$\begin{pmatrix} p_{11} & p_{12} & p_{13} & 0 & p_{15} & 0 \\ p_{21} & p_{22} & p_{23} & 0 & p_{25} & 0 \\ p_{31} & p_{32} & p_{33} & 0 & p_{35} & 0 \\ 0 & 0 & 0 & p_{44} & 0 & p_{46} \\ p_{51} & p_{52} & p_{53} & 0 & p_{55} & 0 \\ 0 & 0 & 0 & p_{64} & 0 & p_{66} \end{pmatrix}$$

Point groups 2, *m*, 2/*m* (2 ∥ x_3)

$$\begin{pmatrix} p_{11} & p_{12} & p_{13} & 0 & 0 & p_{16} \\ p_{21} & p_{22} & p_{23} & 0 & 0 & p_{26} \\ p_{31} & p_{32} & p_{33} & 0 & 0 & p_{36} \\ 0 & 0 & 0 & p_{44} & p_{45} & 0 \\ 0 & 0 & 0 & p_{54} & p_{55} & 0 \\ p_{61} & p_{62} & p_{63} & 0 & 0 & p_{66} \end{pmatrix}$$

Hexagonal

Point groups 6, $\bar{6}$, 6/*m*

$$\begin{pmatrix} p_{11} & p_{12} & p_{13} & 0 & 0 & p_{16} \\ p_{12} & p_{11} & p_{13} & 0 & 0 & -p_{16} \\ p_{31} & p_{31} & p_{33} & 0 & 0 & 0 \\ 0 & 0 & 0 & p_{44} & p_{45} & 0 \\ 0 & 0 & 0 & -p_{45} & p_{44} & 0 \\ -p_{16} & p_{16} & 0 & 0 & 0 & \tfrac{1}{2}(p_{11}-p_{12}) \end{pmatrix}$$

Point groups 6*mm*, $\bar{6}$*m*2, 622, 6/*mmm*

$$\begin{pmatrix} p_{11} & p_{12} & p_{13} & 0 & 0 & 0 \\ p_{12} & p_{11} & p_{13} & 0 & 0 & 0 \\ p_{13} & p_{13} & p_{33} & 0 & 0 & 0 \\ 0 & 0 & 0 & p_{44} & 0 & 0 \\ 0 & 0 & 0 & 0 & p_{44} & 0 \\ 0 & 0 & 0 & 0 & 0 & \tfrac{1}{2}(p_{11}-p_{12}) \end{pmatrix}$$

Cubic

Point groups *m*$\bar{3}$, 23

$$\begin{pmatrix} p_{11} & p_{12} & p_{21} & 0 & 0 & 0 \\ p_{21} & p_{11} & p_{12} & 0 & 0 & 0 \\ p_{12} & p_{21} & p_{11} & 0 & 0 & 0 \\ 0 & 0 & 0 & p_{44} & 0 & 0 \\ 0 & 0 & 0 & 0 & p_{44} & 0 \\ 0 & 0 & 0 & 0 & 0 & p_{44} \end{pmatrix}$$

Point groups $\bar{4}$3*m*, 432, *m*$\bar{3}$*m*

$$\begin{pmatrix} p_{11} & p_{12} & p_{12} & 0 & 0 & 0 \\ p_{12} & p_{11} & p_{13} & 0 & 0 & 0 \\ p_{12} & p_{12} & p_{11} & 0 & 0 & 0 \\ 0 & 0 & 0 & p_{44} & 0 & 0 \\ 0 & 0 & 0 & 0 & p_{44} & 0 \\ 0 & 0 & 0 & 0 & 0 & p_{44} \end{pmatrix}$$

Isotropic

$$\begin{pmatrix} p_{11} & p_{12} & p_{12} & 0 & 0 & 0 \\ p_{12} & p_{11} & p_{13} & 0 & 0 & 0 \\ p_{12} & p_{12} & p_{11} & 0 & 0 & 0 \\ 0 & 0 & 0 & \tfrac{1}{2}(p_{11}-p_{12}) & 0 & 0 \\ 0 & 0 & 0 & 0 & \tfrac{1}{2}(p_{11}-p_{12}) & 0 \\ 0 & 0 & 0 & 0 & 0 & \tfrac{1}{2}(p_{11}-p_{12}) \end{pmatrix}$$

$$\Delta n_1 = \Delta n_2 = -\frac{n_{\rm cub}^3}{2} p_{12} S_3^s$$
$$\Delta n_3 = -\frac{n_{\rm cub}^3}{2} p_{11} S_3^s, \qquad (1.6.7.9)$$

where $n_{\rm cub}$ is the refractive index of the cubic phase. Thus the birefringence in the tetragonal phase as seen by light travelling along x_1 is given by

$$\Delta n_3 - \Delta n_2 = -\frac{n_{\rm cub}^3}{2}(p_{11} - p_{12}) S_3^s. \qquad (1.6.7.10)$$

Thus a direct connection is made between the birefringence of the tetragonal phase of $BaTiO_3$ and its lattice parameters *via* the spontaneous strain. As in the case of the linear electro-optic effect, the calculation can be repeated using equation (1.6.3.14) with the susceptibilities χ_{11} and χ_{12} to yield the relationship

$$p_{11} = \frac{c_{1111}\varepsilon_o \chi_{11}}{n_o^4}; \quad p_{12} = \frac{c_{1122}\varepsilon_o \chi_{12}}{n_o^4}. \qquad (1.6.7.11)$$

1.6.7.3. *The acousto-optic effect*

The acousto-optic effect (Sapriel, 1976) is really a variant of the elasto-optic effect, in that the strain field is created by the passage of a sound wave through the crystal. If this wave has frequency ω_1, the resulting polarization in the presence of a light wave of frequency ω_2 is given by $P_i^\omega = \chi_{ijk\ell} E_j^{\omega_2} S_{k\ell}^{\omega_1}$, where $\omega = \omega_1 \pm \omega_2$. However, since the sound-wave frequency is very small compared with that of the light, to all intents and purposes the change in frequency of the light field can be ignored. The effect then of the sound wave is to produce within an acousto-optic crystal a spatially modulated change in refractive index: a beam of light can then be diffracted by this spatial modulation, the resulting optical diffraction pattern thus changing with the changing sound signal. Acousto-optic materials therefore can be used as transducers for converting sound signals into optical signals for transmission down optical fibres in communications systems. Consider, for instance, a sound wave propagating along the [110] direction in gallium arsenide (GaAs), which crystallizes in point group $\bar{4}3m$. Suppose that this sound wave is longitudinally polarized. With respect to the cube axes, this corresponds to an oscillatory shear strain $S_{12}\sin(\omega t - k\xi)$, where ξ is a distance along the [110] direction (Fig. 1.6.7.1). Then one can write

$$\Delta\eta_{ij} = p_{ij12} S_{12} \sin(\omega t - k\xi) \qquad (1.6.7.12)$$

or in contracted notation

$$\Delta\eta_i = p_{i6} S_6 \sin(\omega t - k\xi). \qquad (1.6.7.13)$$

From Table 1.6.7.1, it seen that the change in dielectric impermeability tensor is

$$\Delta\eta_6 = p_{66}S_6\sin(\omega t - k\xi) = p_{44}S_6\sin(\omega t - k\xi) \qquad (1.6.7.14)$$

since all other components are zero. This means that the original spherical indicatrix of the cubic crystal has been distorted to form a biaxial indicatrix whose axes oscillate in length according to

$$\begin{aligned} n_1 &= n_{\rm cub} + \frac{n_{\rm cub}^3}{2}p_{44}S_6\sin(\omega t - k\xi) \\ n_2 &= n_{\rm cub} - \frac{n_{\rm cub}^3}{2}p_{44}S_6\sin(\omega t - k\xi) \\ n_3 &= n_{\rm cub}, \end{aligned} \qquad (1.6.7.15)$$

thus forming an optical grating of spatial periodicity given by the $k\xi$ term. In gallium arsenide, at a wavelength of light equal to 1.15 μm, $p_{11} = -0.165$, $p_{12} = -0.140$ and $p_{44} = -0.072$. It is convenient to define a figure of merit for acousto-optic materials (Yariv & Yeh, 1983) given by

$$M = \frac{n^6p^2}{dv^3}, \qquad (1.6.7.16)$$

where v is the velocity of the sound wave and d is the density of the solid. For gallium arsenide, $d = 5340$ kg m^{-3}, and for a sound wave propagating as above $v = 5.15$ m s^{-1}. At the wavelength $\lambda = 1.15\mu$m, $n = 3.37$, and so it is found that $M = 104$. In practice, figures of merits can range from less than 0.001 up to as high as 4400 in the case of Te, and so the value for gallium arsenide makes it potentially useful as an acousto-optic material for infrared signals.

1.6.8. Glossary

α, β, γ	refractive indices of biaxial indicatrix, $\alpha < \beta < \gamma$
$\hat{\boldsymbol{\alpha}}$	polarizability operator
B_i	ith component of magnetic induction
c	velocity of light
$c_{k\ell mn}$	$k\ell mn$th component of elastic stiffness tensor
$\chi_{ijk\ldots}$	$ijk\ldots$th component of generalized susceptibility
d	density
D_i	ith component of dielectric displacement
Δ	phase difference of light
$\hat{e}_{ijm}$	unit antisymmetric pseudotensor of rank 3
E_i	ith component of electric field
g_{ij}, G_{ij}	ijth component of gyration tensor
$\mathbf{G}$	gyration vector
$\gamma_{ij\ell}$	third-rank optical gyration susceptibility
$\mathbf{H}$	magnetic field intensity
η_{ij}	ijth component of dielectric impermeability tensor
ε_o	permittivity of free space
ε_{ij}	ijth component of dielectric tensor
κ	ellipticity of wave
$\mathbf{k}$	wavevector of light propagating in crystal ($\lvert k\rvert = 2\pi/\lambda$)
λ	wavelength of light
μ_o	vacuum magnetic permeability
n	refractive index of light
n_α, n_β, n_γ	refractive indices for biaxial indicatrix, $n_\alpha < n_\beta < n_\gamma$
n_o	ordinary refractive index
n_e	extraordinary refractive index
Ψ_i	wavefunction of state i
P_i	ith component of electric polarization
$p_{ijk\ell}$	$ijk\ell$th component of elasto-optic (strain-optic) tensor
$\hat{p}$	electric dipole operator
ρ	optical rotatory power
$\pi_{ijk\ell}$	$ijk\ell$th component of linear piezo-optic tensor
r_{ijk}	ijkth component of linear electro-optic tensor
$\hat{\boldsymbol{s}}$	unit vector in the direction of **s**, the wave normal
S_{ij}	ijth component of strain tensor
T_{ij}	ijth component of stress tensor
v	velocity of sound
V	half the angle between optic axes
ω	cyclic frequency
x_i	direction of ith Cartesian axis, $i = 1, 2, 3$

References

Agranovich, V. M. & Ginzburg, V. C. (1984). *Crystal optics with spatial dispersion, and excitons*. Berlin: Springer.

Bloss, F. D. (1961). *An introduction to the methods of optical crystallography*. New York: Holt, Rinehart and Winston.

Born, M. (1933). *Dynamische Gittertheorie der Kristalle*. In *Handbuch der Physik*, **24**, 623–794.

Born, M. & Wolf, E. (1993). *Principles of optics*. Sixth corrected edition. Oxford: Pergamon Press. Reissued (1999) by Cambridge University Press.

Bragg, W. L. (1924). *The refractive indices of calcite and aragonite. Proc. R. Soc. London Ser. A*, **105**, 370.

Butcher, P. N. & Cotter, D. (1990). *The elements of nonlinear optics*. Cambridge University Press.

Devarajan, V. & Glazer, A. M. (1986). *Theory and computation of optical rotatory power in inorganic crystals. Acta Cryst.* A**42**, 560–569.

Ewald, P. P. (1916). *Zur Begründung der Kristalloptik. Ann. Phys. (Leipzig)*, **49**, 1–38, 117–143.

Glazer, A. M. (2002). *WINOPTACT: a computer program to calculate optical rotatory power and refractive indices from crystal structure data. J. Appl. Cryst.* **35**, 652.

Glazer, A. M., Lewis, J. G. & Kaminsky, W. (1996). *An automatic optical imaging system for birefringent media. Proc. R. Soc. London Ser. A*, **452**, 2751–2765.

Glazer, A. M. & Stadnicka, K. (1986). *On the origin of optical activity in crystal structures. J. Appl. Cryst.* **19**, 108–122.

Glazer, A. M. & Stadnicka, K. (1989). *On the use of the term 'absolute' in crystallography. Acta Cryst.* A**45**, 234–238.

Groth, P. (1906–1919). *Chemische Kristallographie*. Vols. I-V. Leipzig: Engelmann.

Hartshorne, N. H. & Stuart, A. (1970). *Crystals and the polarising microscope*. London: Arnold.

Jona, F. & Shirane, G. (1962). *Ferroelectric crystals*. Oxford: Pergamon.

Jones, R. C. (1948). *A new calculus for the treatment of optical systems. VII. Properties of N-matrices. J. Opt. Soc. Am.* **38**, 671–685.

Kaminow, I. P. (1974). *An introduction to electro-optic devices*. New York: Academic Press.

Kerr, P. F. (1959). *Optical mineralogy*. New York: McGraw-Hill.

Lines, M. E. & Glass, A. M. (1979). *Principles and applications of ferroelectrics and related materials*. Oxford: Clarendon.

Lowry, T. M. (1935). *Optical rotatory power*. London: Longmans.

Moxon, J. R. L. & Renshaw, A. R. (1990). *The simultaneous measurement of optical activity and circular dichroism in birefringent linearly dichroic crystal sections: I. Introduction and description of the method. J. Phys. Condens. Matter*, **2**, 6807–6836.

Moxon, J. R. L., Renshaw, A. R. & Tebbutt, I. J. (1991). *The simultaneous measurement of optical activity and circular dichroism in birefringent linearly dichroic crystal sections: II. Description of the apparatus and results for quartz, nickel sulphate hexahydrate and benzil. J. Phys. D Appl. Phys.* **24**, 1187–1192.

Narasimhamurty, T. S. (1981). *Photoelastic and electro-optic properties of crystals*. New York: Plenum.

Nussbaum, A. & Phillips, R. A. (1976). *Contemporary optics for scientists and engineers*. New Jersey: Prentice Hall.

Sapriel, J. (1976). *Acousto-optics*. Chichester: Wiley.

Szivessy, G. & Münster, C. (1934). *Über die Prüfung der Gitteroptik bei aktiven Kristallen. Ann. Phys. (Leipzig)*, **20**, 703–736.

Wahlstrom, E. E. (1959). *Optical crystallography*. New York: Wiley.
Winchell, A. N. (1931). *Microscopic characters of artificial inorganic solid substances or artificial minerals*. New York: Wiley. [New edition (1964). New York: Academic Press.]
Winchell, A. N. (1939). *Elements of optical mineralogy, Part III*. New York: Wiley.
Winchell, A. N. (1951). *Elements of optical mineralogy, Part II*. New York: Wiley.
Winchell, A. N. (1954). *The optical properties of organic compounds*. New York: Academic Press.
Winchell, A. N. (1965). *Optical properties of minerals. A determinative table*. New York: Academic Press.
Wood, I. G. & Glazer, A. M. (1980). *Ferroelastic phase transition in $BiVO_4$. I. Birefringence measurements using the rotating-analyser method. J. Appl. Cryst.* **13**, 217–223.
Yariv, A. & Yeh, P. (1983). *Optical waves in crystals*. New York: Wiley.